AD/A-004 156

ANALYSIS OF PERFORMANCE OF IR DETECTORS UNDER RADIATION ENVIRONMENTS

Roland E. Leadon, et al

Intelcom Rad Tech

Prepared for:

Air Force Cambridge Research Laboratories
Defense Nuclear Agency

24 July 1974
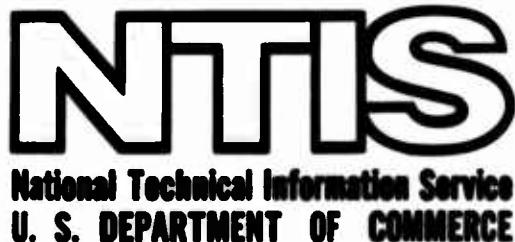
SECURITY CLASSIFICATION OF THIS PAGE *(When Data Entered)*

REPORT DOCUMENTATION PAGE		READ INSTRUCTIONS BEFORE COMPLETING FORM
1. REPORT NUMBER AFCRL-TR-74-0383	2. GOVT ACCESSION NO.	3. RECIPIENT'S CATALOG NUMBER AD/A-004156
4. TITLE *(and Subtitle)* ANALYSIS OF PERFORMANCE OF IR DETECTORS UNDER RADIATION ENVIRONMENTS		5. TYPE OF REPORT & PERIOD COVERED Scientific #2 July 1, 1973-June 30, 1974
		6. PERFORMING ORG. REPORT NUMBER 8028-006
7. AUTHOR(s) Roland E. Leadon, Barry A. Green, Robert A. Berger, and Rodolfo A. Cesena		8. CONTRACT OR GRANT NUMBER(s) F19628-72-C-0349
9. PERFORMING ORGANIZATION NAME AND ADDRESS Intelcom Rad Tech P. O. Box 80817 San Diego, California 92138		10. PROGRAM ELEMENT, PROJECT, TASK AREA & WORK UNIT NUMBERS N/A 627044
11. CONTROLLING OFFICE NAME AND ADDRESS Air Force Cambridge Research Laboratories Hanscom AFB, Massachusetts 01731 Contract Monitor: Mr. Benjamin R. Capone/LQD		12. REPORT DATE July 24, 1974
		13. NUMBER OF PAGES 74
14. MONITORING AGENCY NAME & ADDRESS(if different from Controlling Office)		15. SECURITY CLASS. (of this report) Unclassified
		15a. DECLASSIFICATION/DOWNGRADING SCHEDULE

16. DISTRIBUTION STATEMENT *(of this Report)*

Approved for public release; distribution unlimited.

17. DISTRIBUTION STATEMENT *(of the abstract entered in Block 20, if different from Report)*

18. SUPPLEMENTARY NOTES

This research was sponsored by the Defense Nuclear Agency under Subtask Z99QAXTA026, Work Unit 41, entitled "Radiation Effects in IR Sensors."

19. KEY WORDS *(Continue on reverse side if necessary and identify by block number)*

Photoconductive detectors Computer modeling
Photovoltaic detectors Transient response
Silicon detectors Spiking noise

PRICES SUBJECT TO CHANGE

20. ABSTRACT *(Continue on reverse side if necessary and identify by block number)*

A mathematical computer model has been developed for the transient response of silicon photoconductive IR detectors at low temperatures. Predicted responses are compared to measured time histories resulting from short-pulse Linac excitations. The model is used to predict the response of the detector to single gamma events and to explain the memory effect of a moving IR spot. Future work will utilize the model to investigate the spontaneous spiking noise of biased photoconductive detectors

DD FORM 1473 1 JAN 73 EDITION OF 1 NOV 65 IS OBSOLETE

20

and the response of photovoltaic detectors. Experimental spiking and photovoltaic detector data are presented for use in these analyses.

FOREWORD

This report covers the work performed from July 1973 to July 1974 under contract F19628-72-C-0349 with the Air Force Systems Command, Electronic Systems Division. The work was monitored by Mr. Benjamin R. Capone.

The work at Intelcom Rad Tech (Project 8028) was under the direction of J. A. Naber. The theoretical modeling of the detectors was performed by R. E. Leadon and B. A. Green. The measurements of the spike noise characteristics were made by R. A. Berger, and photovoltaic measurements were made by R. A. Cesena.

CONTENTS

FIGURES

1. SUMMARY

The purpose of this program has been to develop mathematical models to help explain observed phenomena in IR detectors and to predict their responses to various ionization environments. The approach that has been used is to (1) start with experimental data on actual detectors, (2) assume physical models which might explain these data, (3) use the PN code to test whether the models can reasonably approximate the experimental data and to determine the appropriate numerical parameters in the model, and (4) use the models thus determined to predict the detector responses to other radiation conditions and to suggest ways of improving the detector characteristics.

Thus far, most of the work has been on silicon extrinsic photoconductive detectors. In the previous year of this program, some general studies were made to outline the physics of detectors, including contact effects, and to test the ability of the PN code to simulate such detector phenomena as dielectric relaxation and single gamma events. A detailed modeling effort was also begun to determine a model for a silicon extrinsic photoconductive detector that would reproduce the time histories of the response of certain detectors to short Linac ionization pulses. The results of all of these investigations were presented in Reference 1.

During the present year, the model for silicon photoconductive detectors has been tested against similar Linac data for another detector which is presumably a better-quality detector because it exhibits less spiking noise than the first detector. To fit these more recent time histories, it was necessary to modify the original estimates of the model parameters somewhat. However, in spite of the necessity for these modifications, it appears that a reasonably correct physical model for silicon photoconductive detectors has been developed. This model can now be used as a starting point for investigating other detector characteristics. The results of this study are contained in Section 2.2 of this report.

1

This model has also been used to study the response of the detector to single gamma events, to evaluate a possible model for the memory effects of a moving IR spot, and to predict the change in detector response as a function of bias, background illumination, density of counterdoping, and detector size. The computer results indicate that the signal due to a single gamma ray is insensitive to where the ionization from the gamma ray occurs along the length of the detector, provided the same number of electron-hole pairs are created at each location. These results are presented in Section 2.3.1. The model for the moving IR spot successfully predicts a memory effect as a function of the direction of motion of the spot. This model is based on the fact that the excess electrons that are created by the localized spot are swept in one direction by the applied bias. Thus, on the side of the spot in the direction of the electron motion, the electron traps will be more saturated than the traps on the opposite side of the spot. If the spot is moved slowly into the region where the traps are already saturated, the output of the detector will be different than when the spot is moved in the opposite direction — that is, into a region where the traps are less filled. These results are discussed in Section 2.3.2. The predictions of the model for the effect of different operating conditions and detector properties are contained in Section 2.3.3.

Spontaneous noise spiking in photoconductive detectors is known to be a function of the applied bias and probably of the type of contacts to the detector. Since most detector processes, especially contacting techniques, are closely guarded proprietary secrets, one is never sure what the past history of a commercial detector is. Therefore, some simple detectors with gold foil contacts were fabricated at Rad Tech so that we would know how the contacts were made. The spiking characteristics of these detectors, which were made of detector-quality As-doped silicon and which had surprisingly good detector characteristics, were measured as a function of bias, background, and time after application of the light signal. These data are presented in Section 3 and will be used to suggest and test various models for the origin and nature of the spiking.

Much of the work on modeling of silicon photoconductive detectors is also applicable to silicon photovoltaic devices. However, there are enough

2

differences between their characteristics that it is necessary to test the model against data from photovoltaic devices. For this reason, representative silicon photovoltaic detectors were obtained from Electro Nuclear Laboratories and some preliminary data have been taken to characterize these devices. These data, which will be used in developing the photovoltaic model, are presented and discussed in Section 4.

2. MODELING OF SILICON DETECTORS

2.1 Introduction and Background

In the previous year (1972-73), we began by reviewing the physics of detectors and outlining the basic elements of the model for photoconductive detectors, giving special attention to the boundary conditions at the contacts. It was then shown that the PN code correctly simulates dielectric relaxation currents and that simple Shockley-Read recombination theory could explain the main features of the variation of measured detector signals versus temperature. A simplified one-trap silicon detector model was used to demonstrate the effect of localized high densities of dopants at the contacts on the steady-state photoconductive signals.

To get a more realistic detector model, we then used detector time histories resulting from short Linac pulses on a silicon n-type detector (which were obtained under another program), and simulated these responses with the PN code. It was soon clear that the one-trap model could not explain the measured responses since the time histories showed at least two distinct time constants. At low doses, a long rise time ($\sim$1 msec) dominated the response. As the dose was increased, the relative effect of this slow time constant decreased and the faster response time became more prominent. A good fit to several time histories was obtained by using a model which included an attractive donor trap characterized by a slow emission rate and a very shallow acceptor level with a fast emission rate. A set of parameters was obtained to fit the Linac results, and this model was then used to predict detector responses to a gamma event.

During the current work period (1973-74), more modeling of these same Linac results was performed. This additional work was motivated by the observed nonlinear field (or bias) dependence of the photoconductivity (PC) response. This nonlinearity seemed to be related to the fact that the fields were high and the field variations large, from 90 to 720 V/cm. Thus, it

4

appeared that lattice excitation or multi-level trapping states might be causing large variations in carrier velocity and capture cross sections, respectively. Consequently, the mobility and attractive capture cross sections were varied within limits as a function of bias in an attempt to obtain better agreement between calculation and experiment for the bias dependence of the sample. These changes produced improved fits to the results at most doses and fields; however, it was concluded that some of the experimental results were affected by spiking, or some other spurious effects, rendering an exact prediction of all the responses unlikely. This analysis is briefly presented in Section 2.2.1.

At about this time, Linac time histories became available for another, presumably less noisy, detector and it was decided to test the validity of our model on these data. To obtain a good fit, it was found that we had to alter the first set of parameters. Also, this detector did not show the slow rise time characteristic of the deep trap which was so prominent at low doses for the first detector. The fields in the new detector were low compared to the original detector and the response was fairly ohmic; that is, the peak signals were nearly linear with applied bias. Using a one-trap model, we found a set of parameters that well described this low-field detector. This analysis is presented in Section 2.2.2. Then we proceeded to use the model to predict detector responses for different operating conditions and detector parameters, such as: a single gamma event, a moving spot of infrared light, large fields, and different background illuminations, counterdoping densities, and detector sizes. These effects were simulated with the PN code using the one-trap detector model, and the results are presented in Section 2.3.

2.2 Silicon Photoconductivity Detectors

As discussed in Section 2.1, some additional work was required in the modeling of the original detector due to the high fields used during the Linac tests. This analysis will be discussed in Section 2.2.1. The model was also tried on the Linac results of another detector which became available. These latter tests were at lower fields and were believed to be more reliable. These results will be presented in Section 2.2.2.

2.2.1 High-Field Detector

The computer modeling for the PC response of this detector to Linac pulses was presented in Reference 1. The fields in this detector were relatively high and the field variation large, from 90 to 700 V/cm, and this appeared to cause non-ohmic field dependence.

In an attempt to fit the bias dependence of this detector, the capture cross sections (lifetimes) and the mobilities were varied as a function of field in the present work. Norton (Ref. 2) has suggested that the capture cross sections should decrease superlinearly with increasing field at fields $\gtrsim 10^2$ V/cm. Theoretically, this result is based on Lax's cascade model of electron capture (Ref. 3), in which the lower-energy carriers can be trapped in highly excited trap levels, which have orbits of larger radii. Also, it is well known that carrier velocity in a semiconductor saturates with increasing field due to the effect of lattice excitation, producing a large decrease in mobility, μ. For a given phonon excitation energy, the field at which saturation occurs decreases with increasing mobility (Ref. 4). For $\mu = 10^4$ cm^2/V-sec, this decrease can be significant at a few hundred volts/cm for the lattice modes in silicon. The computer modeling in Reference 1 was done under the assumption that the mobility and capture cross sections were independent of the field. These calculations and the experimental curves are summarized in Figures 1, 2, and 3 for various doses. It is evident that the model which gives reasonable agreement with the low-field results does not agree with the high-field points. In these figures, the observed signals increase sublinearly with bias, which may be indicative of a decrease in mobility with field, as discussed above. Also, there appears to be a marked increase in response time with field, perhaps indicative of the field dependence of the carrier lifetime mentioned above.

If one neglects for a moment the high-field, low-dose response of Figure 1 — i.e., 21.7-volt bias at 1.1-mrad/pulse — a suitable variation of mobility and lifetime with applied field gives a somewhat improved fit to the responses. The assumed field dependences of mobility and lifetime are shown in Figure 4 and are seen to be in qualitative agreement with the theory presented above. The resulting improvement in the simulation at the various doses is evident from Figures 1, 2, and 3 and from the response

6
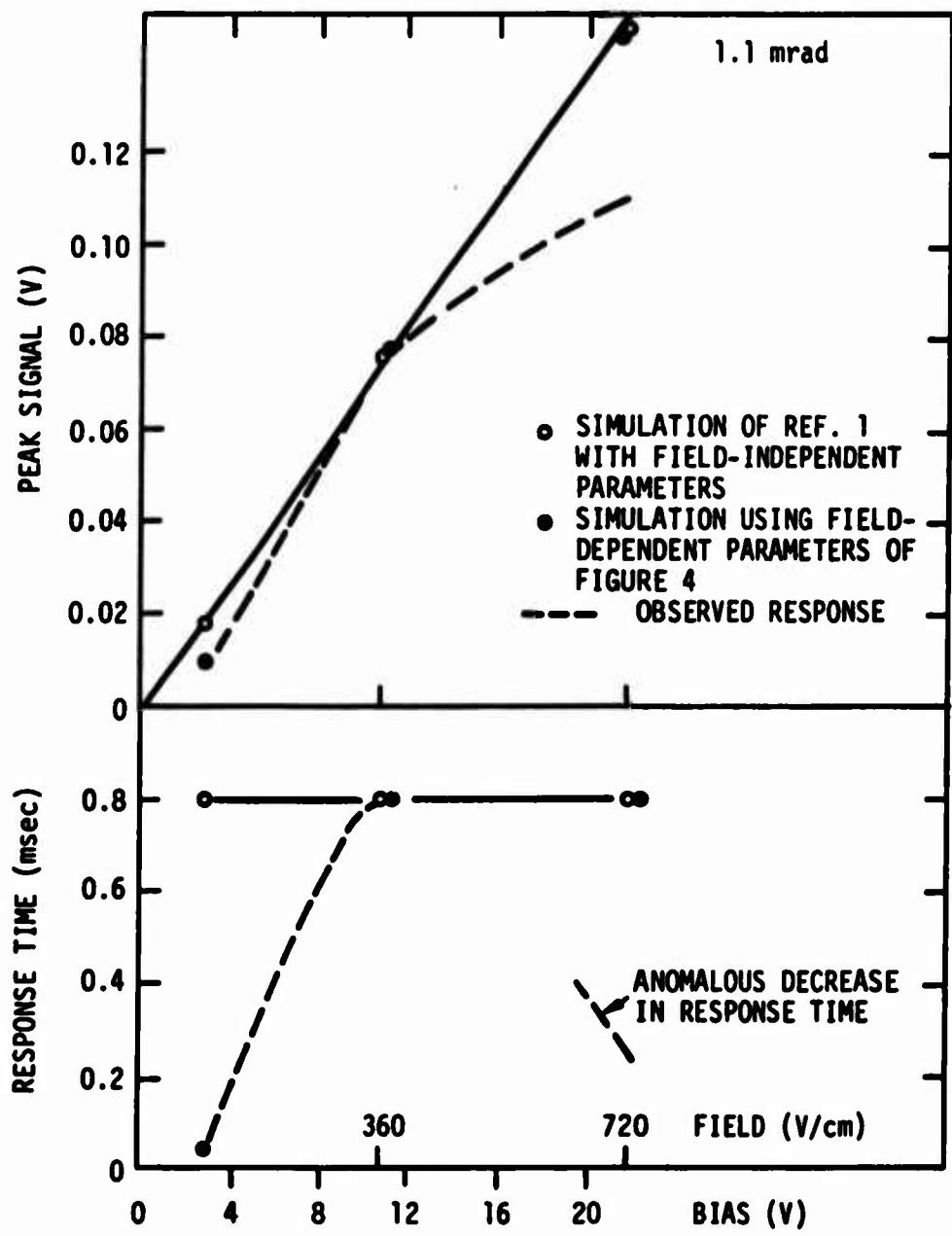
Figure 1. Variation of detector response with field at low dose
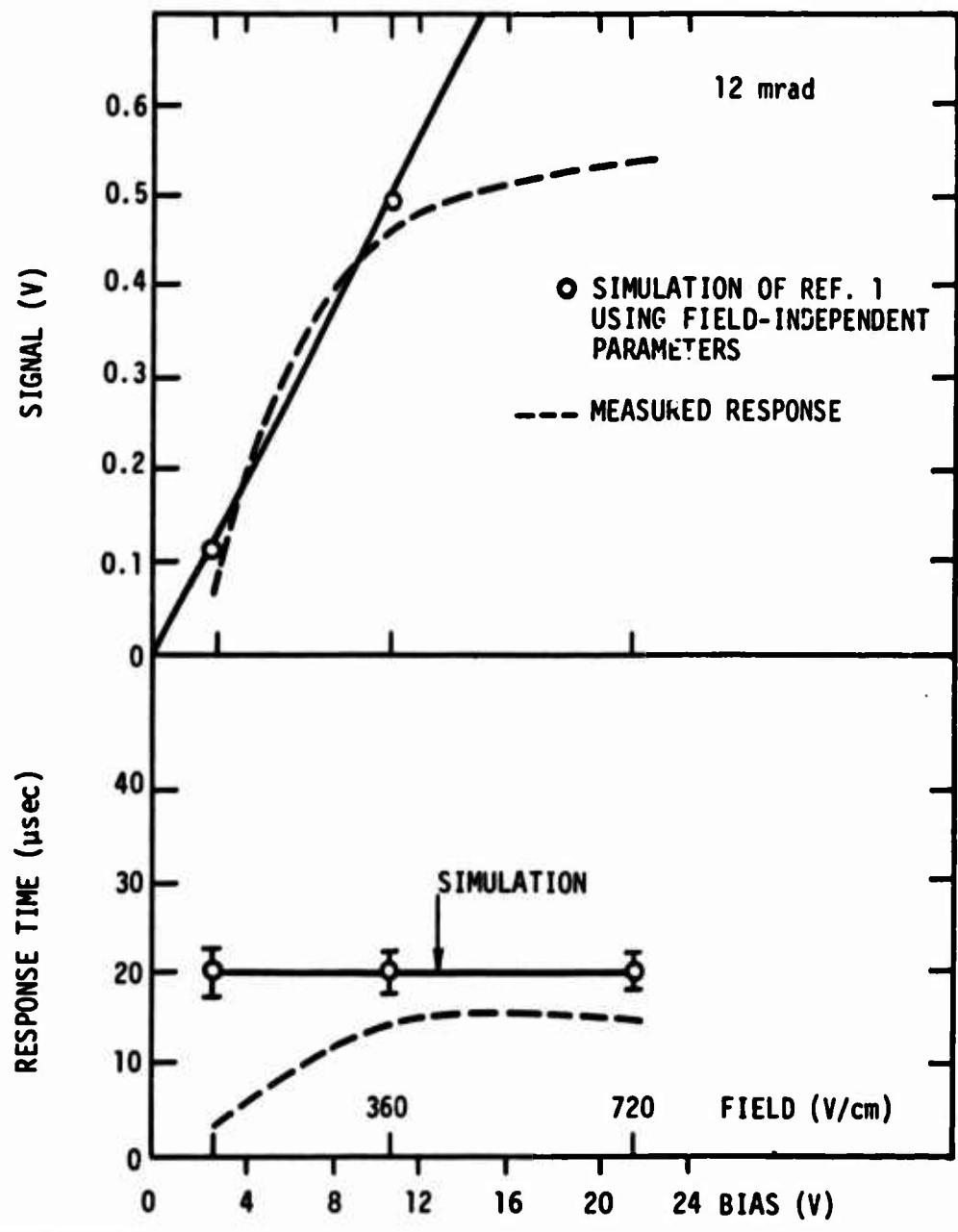
RT-08582

RT-08583

Figure 2. Variation of detector response with field at intermediate dose

8
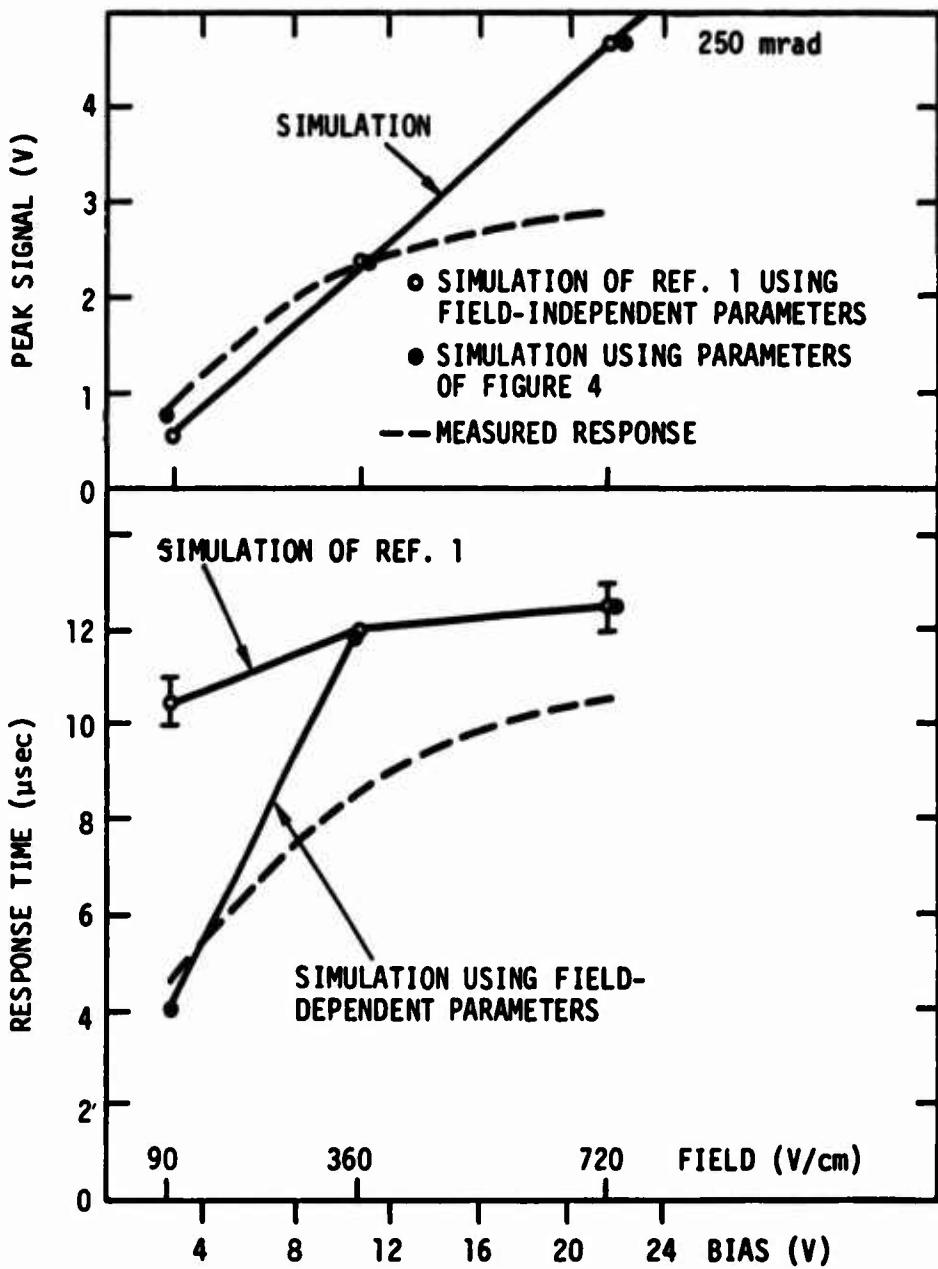
Figure 3. Variation of detector response with field at high dose

RT-08584
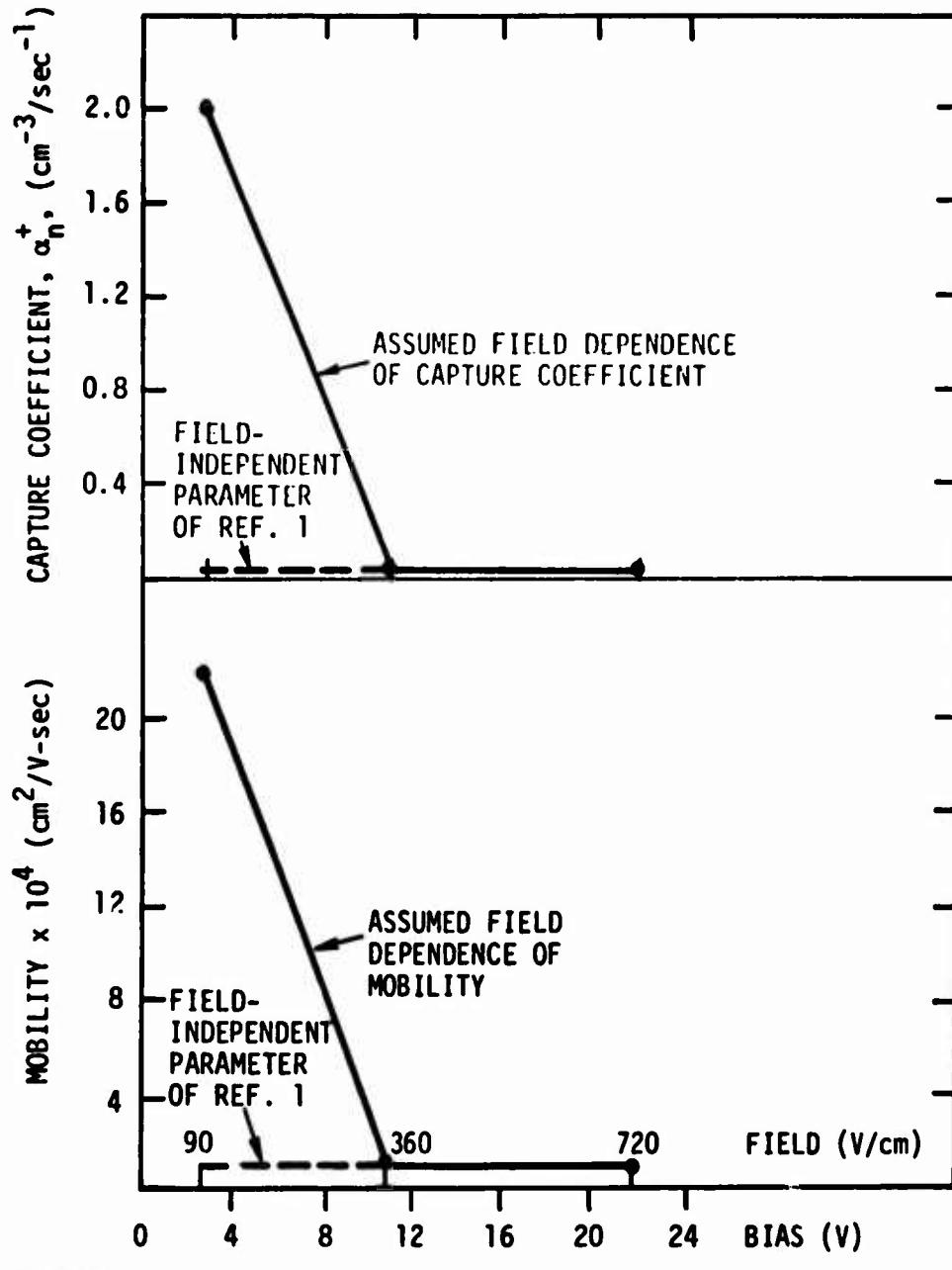
Figure 4. Field variation of mobility and capture coefficient used in model calculations

RT-08585

curves of Figures 5, 6, and 7. Note that, from Figure 4, the assumed field dependence of the mobility and lifetime produces changes from the simulation of Reference 1 only at low fields. The field variations in response are also plotted in Figures 8 and 9, along with the results for the low-field detector, to show the general trends in the effect of the field over a wide variation of operating conditions.

The abovementioned discrepancy at low dose and high field (Figure 1), in which the lifetime appears to reach a maximum and then decrease, does not appear to be a phonon-emission effect since it does not occur at the larger doses. It is possible that, at the high field, spiking occurred. In fact, it is now known that the high-field detectors are subject to spiking. This possibility renders the Linac results for this detector unpredictable with respect to the present model, especially in the result at the highest field, where the field dependence is not consistent with a believable lifetime theory. However, it does appear that the high-field response in Figure 1 is consistent in the velocity saturation, and this is a reasonable behavior. It was concluded that further refinements to the modeling were impractical, and it was decided to concentrate on the low-field detector.

2.2.2 Low-Field Detector

The low-field detector is about 2.5 times longer between contacts than the high-field detectors, and its operating voltage range is 3 to 4 times lower. Thus, the average applied electric field is less by about a factor of 10. The Linac tests were performed at about 12°K, compared to 10°K for the high-field detector. In addition, due to a light leak, the tests were at a relatively high background intensity where the resistance of the detector was about equal to the load resistance. The effect of these differences — in particular, the background intensity — will be investigated in the model.

The results in Figure 8 indicate that the response of the new detector is essentially linear with bias (within the accuracy of the data) over its operating range. Since the model predicts practically a linear bias dependence for the signal when the parameters are independent of bias, fitting of the peak signals at other biases is automatically accomplished when the data for one bias are matched. (There should be a slight nonlinearity due to sweep-out effects, but this effect is small for the present operating conditions because the sweep-out time is large compared to the recombination

11
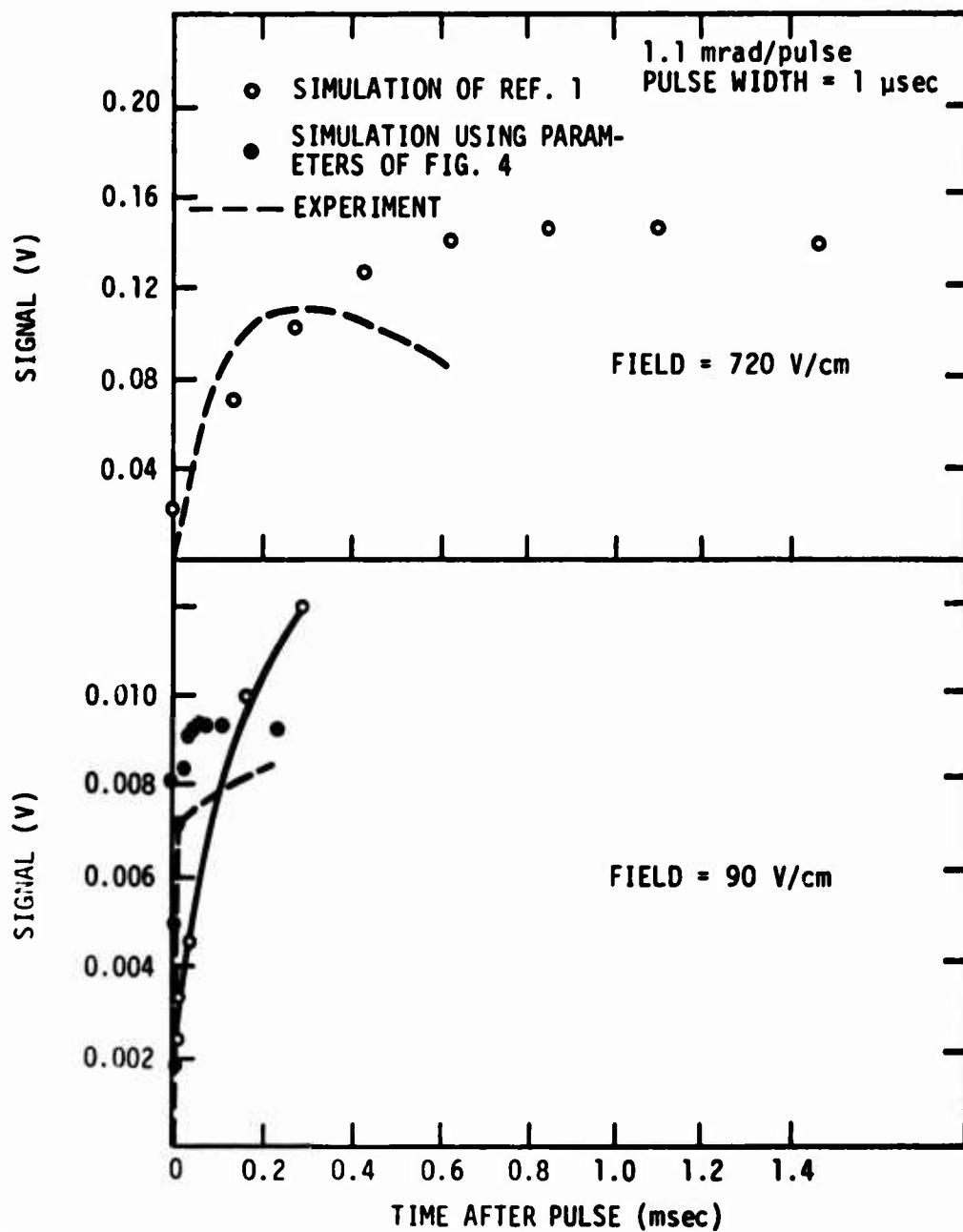
RT-08586

Figure 5.   Photoconductivity response of high-field detector at low dose
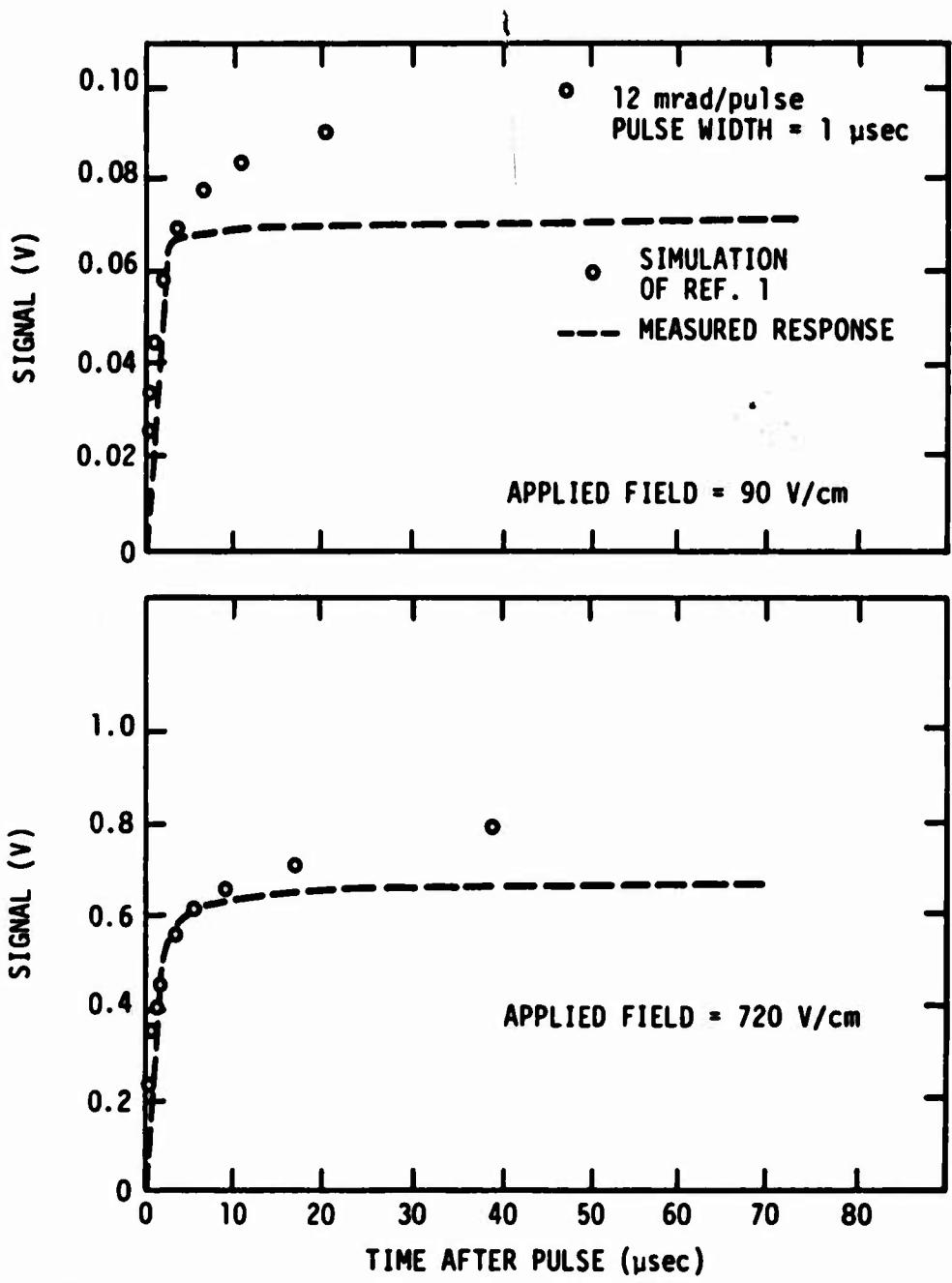
RT-08587

Figure 6. Photoconductivity response of high-field detector at intermediate dose

13

250 mrad/pulse
PULSE WIDTH = 1 µsec

FIELD = 720 V/cm

--- OBSERVED
o SIMULATION OF REF. 1
● SIMULATION USING
FIELD-DEPENDENT
PARAMETERS OF FIG. 4

FIELD = 90 V/cm

TIME FOLLOWING PULSE APPLICATION (µsec)
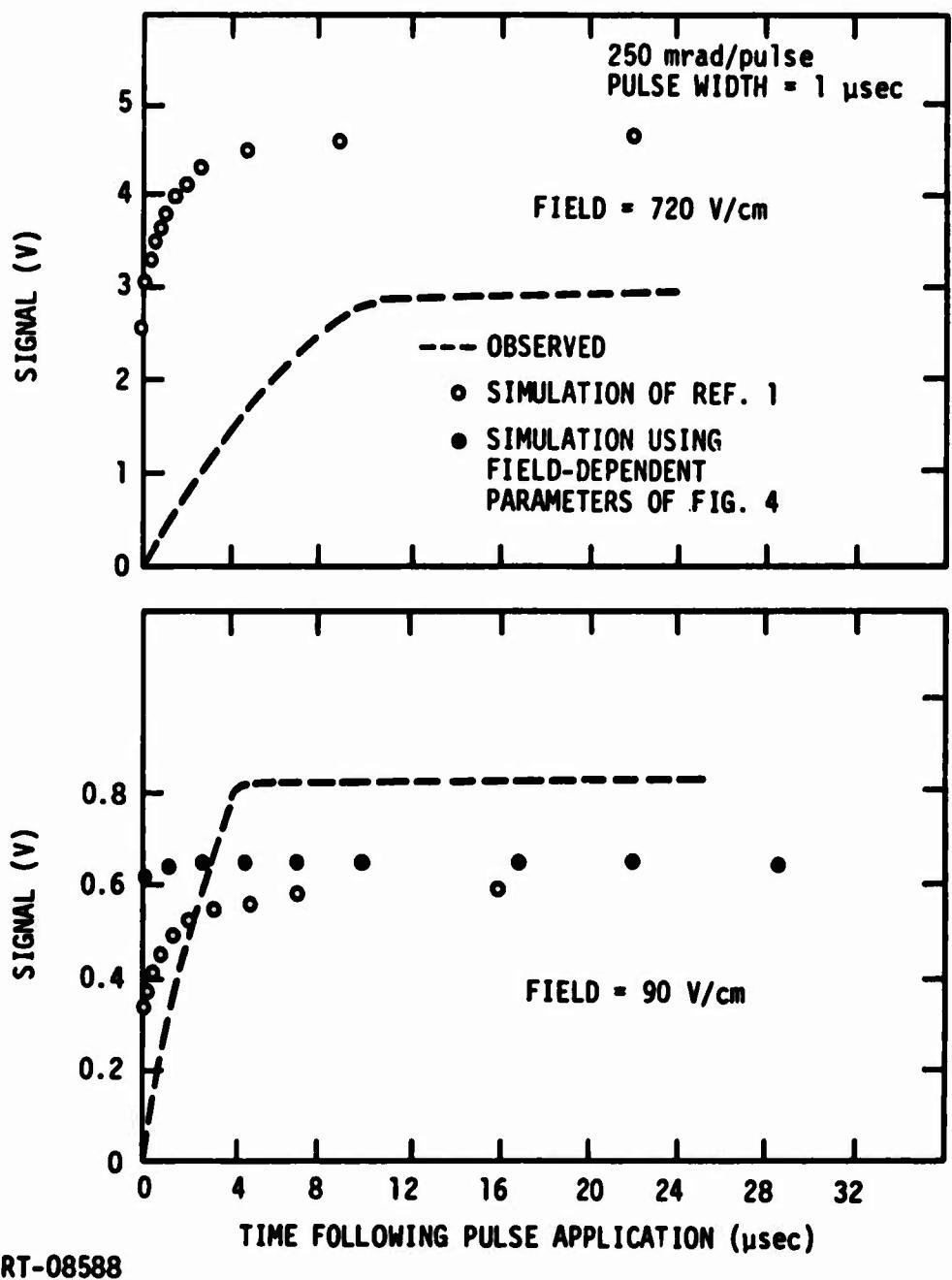
RT-08588

Figure 7.   Photoconductivity response of high-field detector at high dose

14
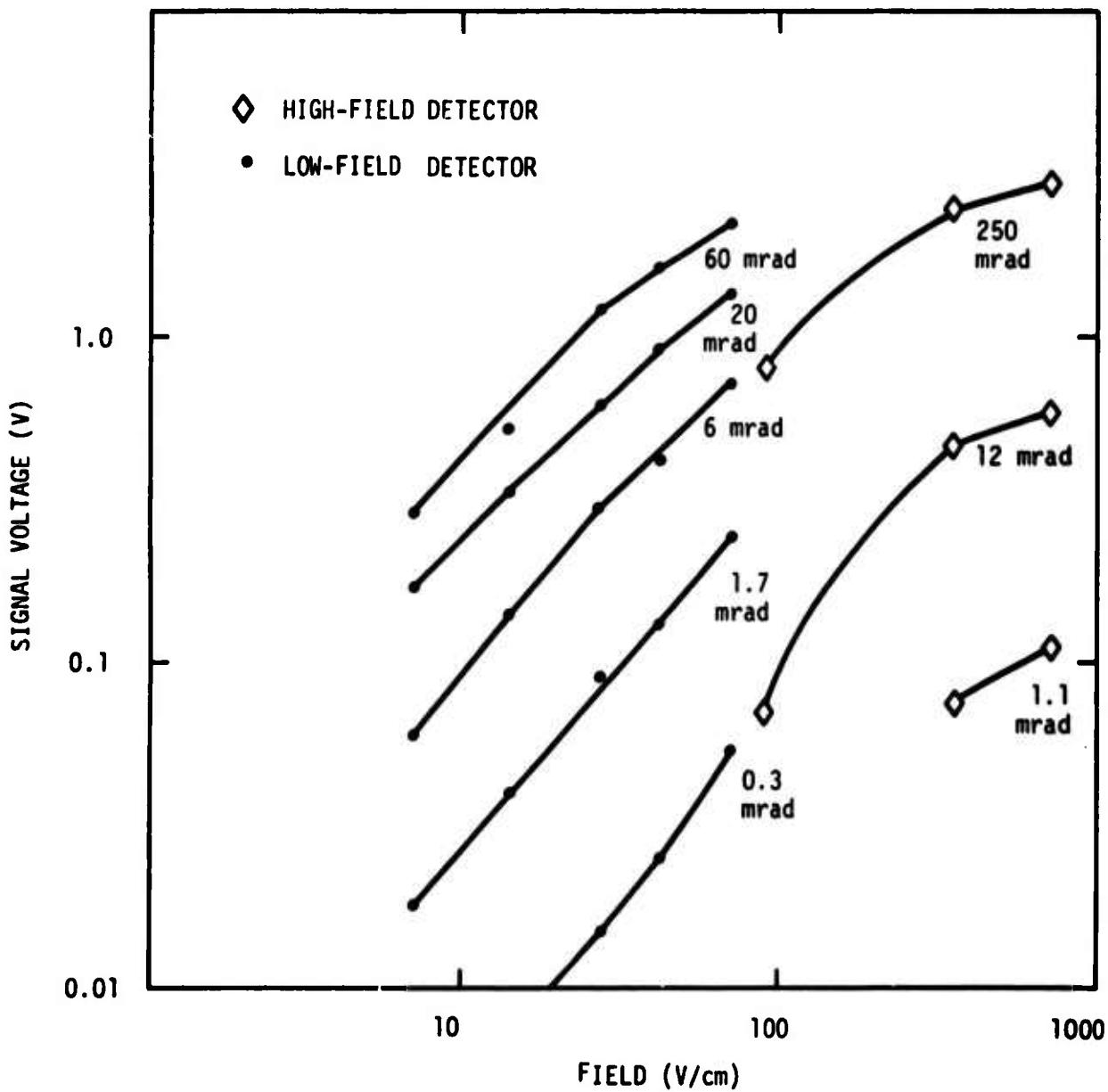
RT-06493

Figure 8. Peak signal versus bias for several doses/pulse for high- and low-field detectors
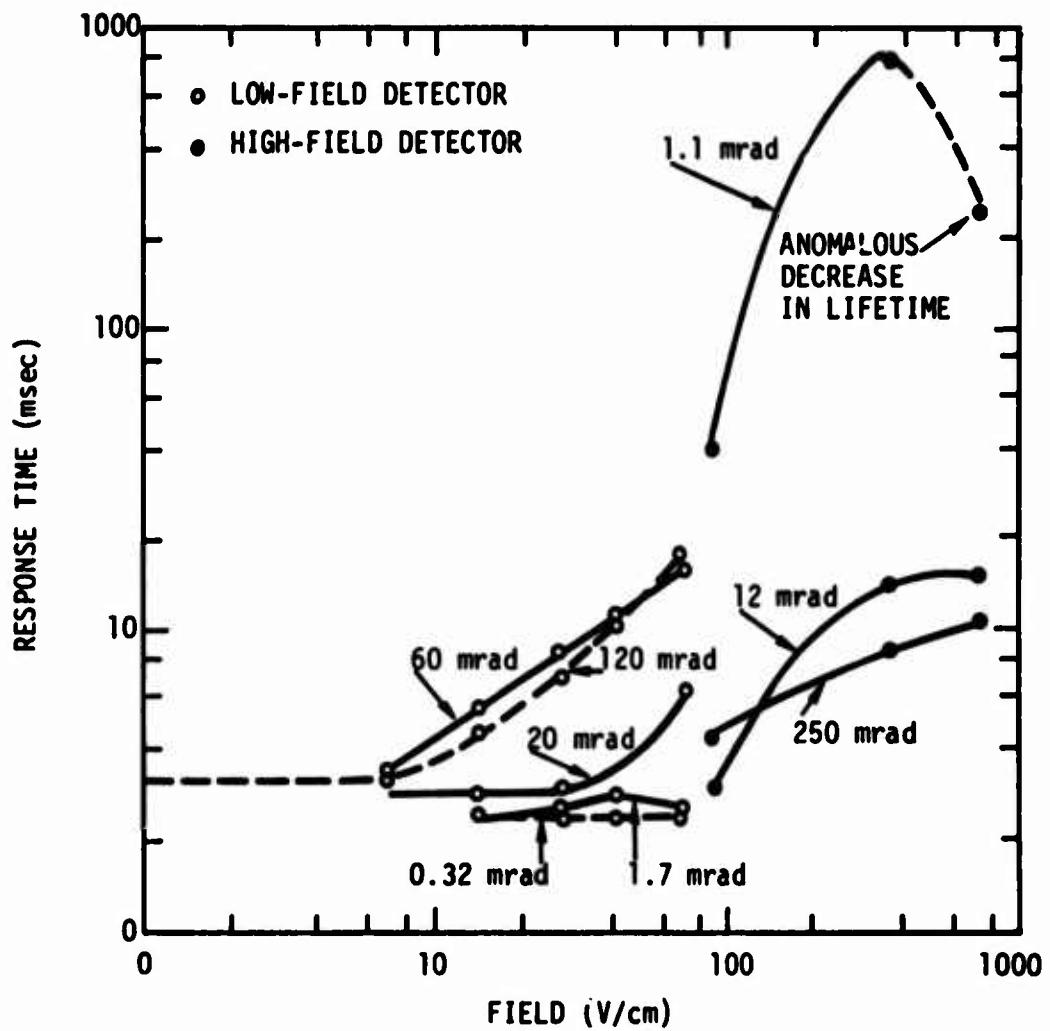
RT-08589

Figure 9. Observed response time variation with field for both detectors

time.) It will also be noted in Figure 8 that the major nonlinearity for the high-field detector occurs at fields considerably above the test range for the low-field detectors. In addition, at the same average field the response per dose is considerably greater for the new detector. The reason for this latter difference is discussed below.

The lifetime variations with field shown in Figure 9 for both high- and low-field detectors are in qualitative agreement, generally showing a rise with bias, and the lifetime analysis given in Section 2.2.1 probably applies to the new detector also.

In contrast to the results in the first detector, this second detector showed very little of the slow response. Most of its signal occurred in a few microseconds, similar to the results for the first detector at large doses. In the model for the first detector, the slow response resulted from a defect donor level between the conduction band and the arsenic donor level which captured electrons and then re-emitted them rather slowly. Two reasons have been suggested for the absence of the slow response in the second detector. First, the density of the trap might be considerably smaller than in the first detector, and thus, the amplitude of its effect could be lost in the remaining response of the detector. The second possible reason is that the higher background intensity that was used in the experiments on the second detector due to the inadvertant light leak could have saturated the trap and thus made it ineffective during the pulsed responses. Computer simulations have not been conclusive enough to determine if either, or perhaps both, of these causes are responsible for this difference between the two detectors. Because the slow response in the first detector is overshadowed by other effects at all but the smallest doses, it was decided to omit this trap from the remaining calculations with this model. If future work should indicate that this trap is important for some situations, it can be returned to the model.

When the fit to the data for the second detector was first started, an attempt was made to use the same physical parameters, such as capture coefficients and trap emission rates, as were obtained from simulating the first detector because these parameters should be fundamental quantities that are not affected by how the detector was fabricated, its densities of

impurities, and the background illumination. Unfortunately, this procedure was not successful. Using the previous capture coefficients and emission rates, we could not find a set of trap and counterdoping densities which gave an adequate fit to the data for the new detector. One possible reason for this difficulty is that a deliberate change was made in the models for the first and second detectors. In the first detector, the very shallow trap was given a rather arbitrary, fairly large density of 1×10^{15} cm^{-3}. When it was later decided that this fast trap is actually another shallow level of the arsenic defect (with an actual density of about 5×10^{16} cm^{-3}), the fit to the data for the first detector was not repeated with this higher density. It was reasoned that an almost identical fit would be obtained with the larger trap density and a correspondingly smaller capture cross section and larger emission parameter, so that the capture and emission rates would remain the same. This is the procedure that was first attempted with the second detector; the trap density and the emission parameter n_1 in the Shockley-Read formula were increased by a factor of 30, and the electron capture coefficient by the neutral, shallow trap ($\alpha_{n_2}^0$) was reduced by the same factor. However, the results were not in good agreement with experiment and other changes were necessary, as discussed below.

The dose dependence of the peak amplitudes is shown in Figure 10, and the final best-fit time histories are given in Figure 11. Parameters for the high-field detector and the final parameters for the low-field detector are compared in Table 1. For the shallow trap, the capture time $(\alpha_{n_1}^0 N_1)^{-1}$ has been kept the same for both detectors. If N_1 is considerably different in the two detectors, this could be a source of the difference. To fit the data with this value of capture time, the re-emission time had to be considerably faster for the new detector. This also accounted for the larger response per dose at a given field for the new detector (see Figure 8). Also, the coefficient for capture of electrons by the positive arsenic donors is smaller for the new detector. A possible reason for these differences was a slightly higher temperature ($\sim 12^\circ$K) during the tests with the new detector compared to a temperature of about 10°K for the original detector. However, this temperature difference does not appear large enough to explain the changes in the parameters. Another possibility is that the

18
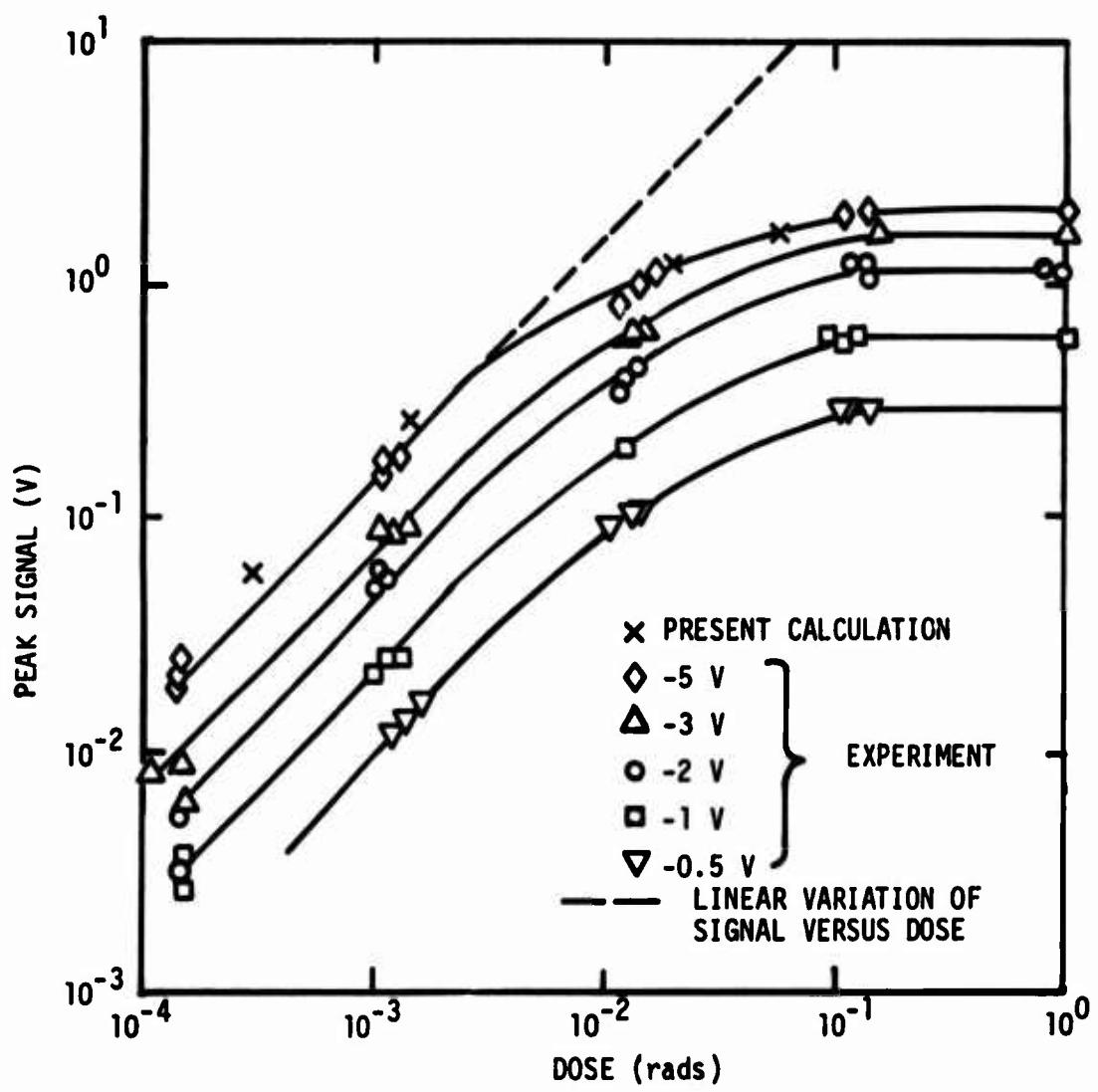
RT-06492

Figure 10.   Peak signal versus Linac dose/pulse for
low-field detector

19
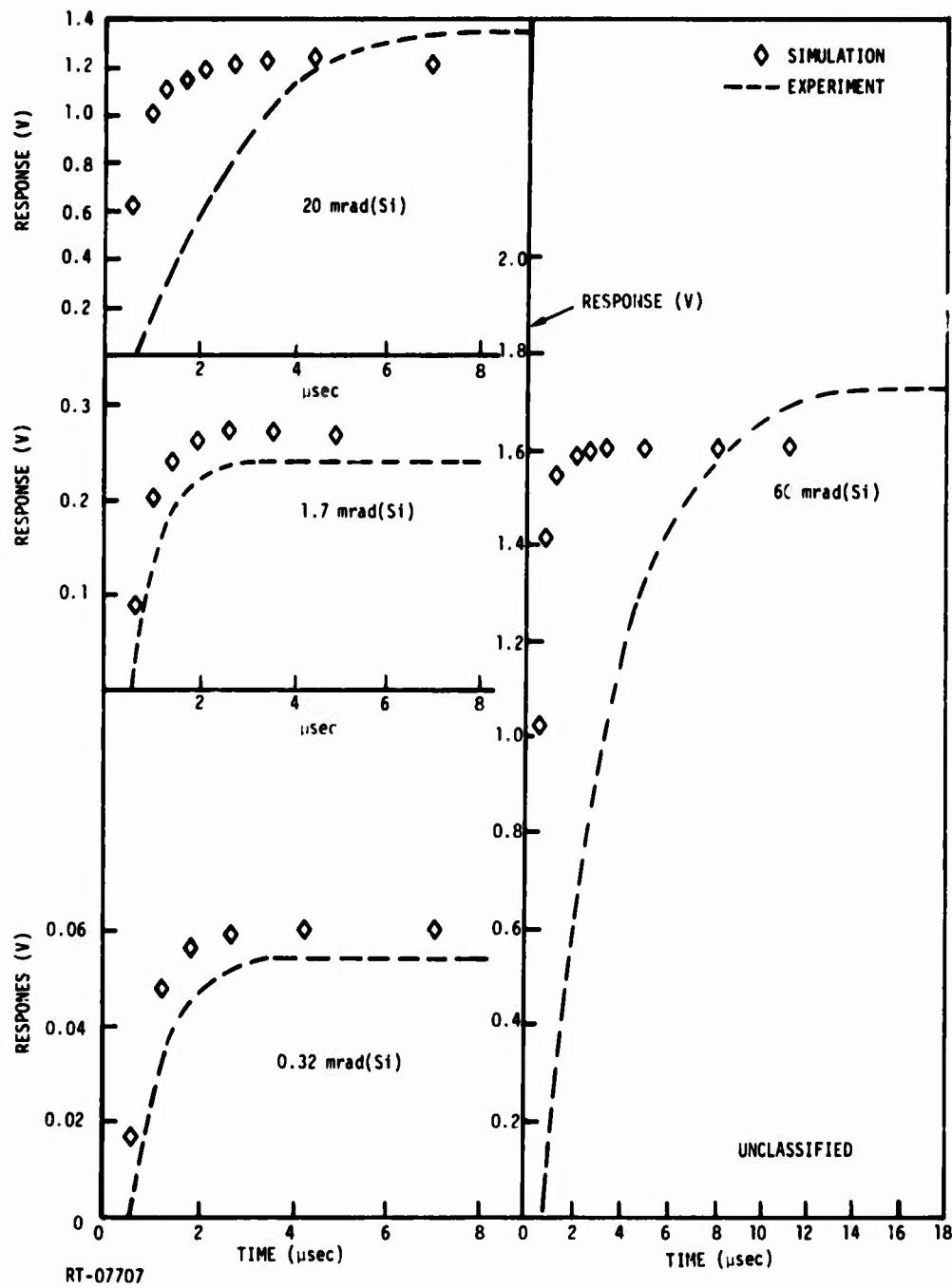
Figure 11. Time histories of signals from low-field detector following 0.2-μsec Linac pulses with various doses (5 V bias)

TABLE 1. COMPARISON OF MODEL PARAMETERS FOR THE TWO SILICON PHOTOCONDUCTIVE DETECTORS

	Original Detector (Ref. 1)	Final Choices for New Detector
Shallow Trap (Neutral Acceptor)		
Density, N_1 (cm^{-3})	1×10^{15}	5×10^{16}
Coefficient for capture of electrons by neutral defect, $(\alpha_{n_1}^0)$ $(cm^{-3}sec^{-1})$	3×10^{-3}	6×10^{-5}
Re-emission time for electrons, $[\tau_{em_1} = (\alpha_{n_1}^0 n_{1,1})^{-1}]$ (sec)	8.3×10^{-9}	8.3×10^{-11}
Deep Trap (Attractive Donor)		
Density, N_2 (cm^{-3})	2×10^{11}	0
Coefficient for capture of electrons by positive defects, $(\alpha_{n_2}^+)$ $(cm^{-3}sec^{-1})$	0.375	-
Re-emission time for electrons, $[\tau_{em_2} = (\alpha_{n_2}^+ n_{1,2}^0]$ (sec)	3.6×10^{-5}	-
Density of counterdopant, N_{cd} (cm^{-3})	4×10^{11}	2×10^{11}
Density of ionized (positive) arsenic atoms in equilibrium (cm^{-3})	2×10^{11}	2×10^{11}
Coefficient for capture of electrons by positive arsenic atoms, $(\alpha_{n_1}^+)$ $(cm^{-3}sec^{-1})$	0.03	0.0033
Electron mobility $(cm^2/V\text{-}sec)$	1×10^4	1×10^4

tendency of the original detector to show spiking at the test biases could significantly alter its response to ionization pulses. And finally, it is always very possible that we have just not succeeded in finding the one set of parameters that will give a good fit for both detectors.

In Figure 10, the signals are linear with dose at low values. The saturation at high doses is partly due to extra recombination through the defects that are ionized by the dose, but mainly because the steady-state resistance of this detector at high background is comparable to the load resistance. Thus, the saturation voltage is about half of the applied voltage. However, in simulating the dose dependence, an initial ionized defect (counterdoping) density had to be found which would yield the correct response amplitude at both high and low doses, since the low-dose region is below the voltage saturation region. This was accomplished by first obtaining the low-dose fit, as described above. Then the recombination cross section and counterdoping density were varied, keeping the ratio of the two nearly constant to leave the low dose response the same (as given by the Shockley-Read formula). For the high-dose response, the ionized defect density was nearly independent of the initial value due to the high hole-injection rate, so that the high-dose response varied with the above ratio (in the absence of voltage saturation). The final computer result, shown in Figure 11, was obtained with the same hole density as for the high-field detector — i.e., a counterdoping of 2×10^{11} cm^{-3} with no attractive donor (see Table 1). As the computed results of Figure 11 are somewhat low at high dose, it is probable that the recombination cross section could have been significantly smaller and the counterdoping correspondingly larger and only a slightly larger (and therefore improved) response obtained in the voltage saturation region.

For present purposes, it does not seem warranted to try further to find one set of parameters that fits both sets of data. Even though the parameters may not be numerically correct for either detector, the basic features of the model appear to be correct, and it is still useful for studying the sensitivity of the detector response to other design changes, such as different densities, etc.

22

It is worth mentioning that still a third detector has been tested with Linac pulses at Rad Tech under another program. The results are similar to those for the first two detectors. In particular, for low doses, the slow rise in the response is again evident, as it was for the first detector. The reason for this could be that this last detector was tested under low backgrounds, similar to the first detector but unlike the second detector which had a light leak.

In summary, three different As-doped silicon detectors have shown comparable responses to Linac pulses. We do not intend to do a detailed simulation of this last detector, but the consistency of the results for the three detectors enhances our confidence in the model.

In Figure 11, the calculated peak amplitudes are in good agreement with experiment. However, the calculated rise times are much faster than experiment, especially at large doses. This same trend was observed in the previous data for the high-field detector, and thus far, no satisfactory explanation has been found for it. Under a different program at Rad Tech, a similar effect was observed when detector-quality bulk silicon was ionized by the Linac or light, and the instantaneous conductivity was measured by a microwave reflection technique. In these experiments, with doses of 1 to 10 rads, the excess conductivity during the pulse was very small and then, after the pulse, the conductivity increased slowly to a maximum and then decayed away. The time for the conductivity to reach a peak became longer with larger doses, similar to the rise time observed in detectors. Thus far, we have not been able to successfully model these data either, so there is probably some feature missing from the model which causes this effect. However, for detector responses, inaccuracies in simulating this slow rise may not be important as long as the peak signals are reasonably correct.

2.3 Prediction of the Model

In this section we use the model developed in Section 2.2.2 to predict detector response to different operating conditions such as a gamma pulse or a moving spot of infrared light. Also of interest are the effects of environment, such as background illumination, on the response. The effect

of operating conditions such as large biases are also investigated, along with the effect of properties controlled by fabrication — e.g., counter-doping density and distance between contacts. All of these effects were simulated with the PN code, using the one-trap detector model which was developed using the low-field detector.

2.3.1 Response to Gamma Spike

The model for the low-field detector was used to study the effects of single gamma events occurring at various locations between the detector contacts. The gamma event was simulated by a short pulse ($\sim 10^{-10}$ sec) of ionization which creates 2×10^5 electron-hole pairs in a narrow region ($\sim 8 \times 10^{-3}$ cm wide) at various locations along the device. A typical time history of the output current using a fast ($\sim 10^{-9}$ sec) RC time constant of the system is shown in Figure 12. The highest point plotted at time zero is the current at the end of the pulse. This current quickly decreases as the electrons are trapped on the shallow traps. The long decay is due to re-emission of electrons from these traps. In a practical situation, one would never see the first fast decrease because the RC of the system is usually too slow. However, it should be possible to observe the slow decay with suitable equipment. The effect of large and small time constants on the response was shown in the previous work period (Ref. 1).

The curve in Figure 12 is the result when the gamma event occurred mid-way between the contacts and one-quarter of the length from the negative contact. The reason that these two positions give identical results is that the transit time for electrons to traverse the full detector is about 10^{-7} sec, whereas the recombination lifetime is $(\alpha_{n_1}^+ N_{cd})^{-1} \simeq 1.6 \times 10^{-9}$ sec, where N_{cd} is the density of overcompensation. Therefore, unless the gamma event occurs very close to the positive contact, all of the electrons will recombine before they reach the contact and the output signal will be independent of the position of the gamma event along the detector. This conclusion greatly simplifies any pulse-height predictions because one variable — namely, the position of the event along the detector — can be eliminated.

24

RT-07711
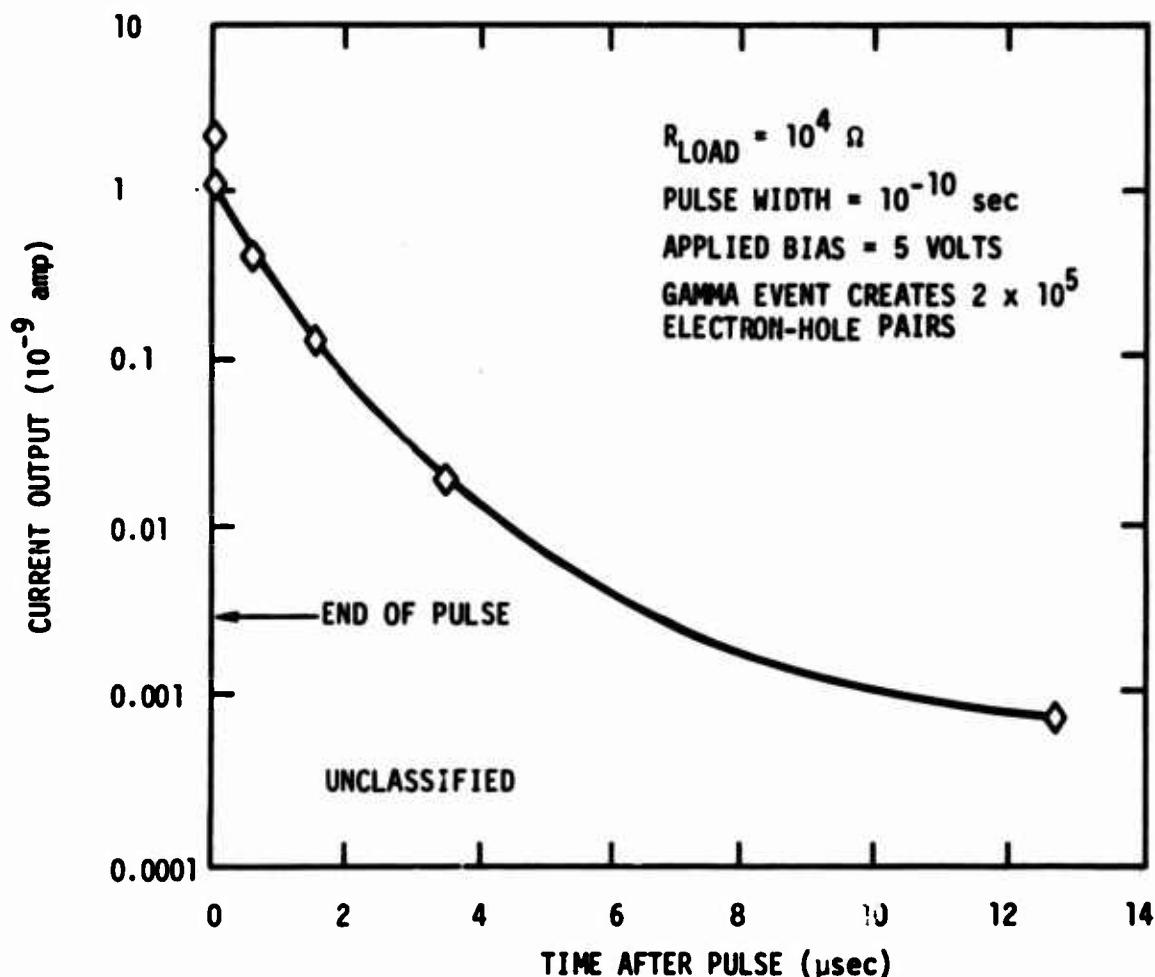
Figure 12. Time history of output current for low-field detector fol-
lowing a single gamma event in interior of detector

2.3.2 Memory Effect of Moving IR Spot

At detector conferences (Ref. 5), it has been reported that silicon extrinsic photoconductive detectors exhibit a memory effect when a small spot of steady IR light is moved over the surface of the detector. In one set of experiments, the spot was initially stationary and the detector output signal increased slowly, on a time scale of seconds, and approached a saturation value. When the spot was then moved to a new region on the detector, the signal dropped back to essentially its previous initial value and then increased toward the same saturation limit. This process was repeated each time the spot was moved to a new region. In another set of experiments, the IR spot was moved slowly between the contacts of the detector. It was found that the output signal was different, depending on whether the spot was moving with or against the applied electric field.

Both of these effects can be explained by the above model of silicon photoconductive detectors. The IR light excites electrons from the neutral donors to the conduction band. These electrons are attracted toward the positive contact and they continue moving in that direction and contribute to the output signal until they are captured by other ionized donors. At low temperatures, the re-emission time for these electrons is very long, so they essentially remain trapped for the duration of the experiment.

When the stationary spot is first turned on, the electrons that are swept away from the spot all encounter virgin material with the equilibrium density of ionized donors and, therefore, a given capture lifetime. However, as time goes on, the ionized donors near the spot become filled with electrons, so the subsequent electrons must travel further before they are captured. Thus, their lifetime is longer and the resulting output signal increases with time. Eventually, the density of ionized donors under the spot becomes large enough that the local recombination lifetime becomes short and the signal no longer increases.

A similar explanation applies to a slowly moving spot. If the spot moves in the direction of the drifting electrons, it is continually moving into a region where some electrons have already been captured and the lifetimes are longer than normal. In this case, the output signal should be larger than when the spot moves opposite to the drifting electrons because,

26

in the latter case, the spot would be always moving into virgin material with a shorter lifetime.

This model was tested on the PN code. A narrow stationary spot of IR light has been simulated, and the time history of the response signal is shown in Figure 13. For convenience in computation, an ionization rate due to the IR light was chosen such that the signal would approach saturation in a few microseconds. This ionization rate is much larger than normal but, for smaller ionization rates, the time scale can just be increased inversely with the ionization rate. This is equivalent to plotting the time history versus total number of generated electrons.

As expected, the magnitude of the signal increased with time and reached a maximum value. However, the computed signal then starts to decrease slowly. This decrease is due to a reduction in the local electric field near the spot which results from the buildup of positive charge from the ionized donors. Since this decay has apparently not been observed in experiments, its magnitude is probably much less in actual experiments than in these calculations. The following are possible reasons for this discrepancy. In an actual device, there is some re-emission of holes from the ionized donors, whereas this re-emission rate was set to zero for the calculations. It is possible that the density of ionized donors finally reaches a point where the re-emission rate for holes equals the ionization rate for creating new ionized donors and the local electric fields do not decrease beyond a certain point. Also, if the background intensity is larger than has been simulated in this example, these excess carriers will tend to be captured by the ionized donors and thus smooth out the distribution of trapped charge. Finally, a more likely explanation is the difference between the simulated one-dimensional problem and the actual approximately two-dimensional experiment. In two dimensions, the electric field due to the charge trapped near the spot will radiate outward from the spot in the plane of the detector, and the local reduction in the field will be much less than was calculated in one dimension. If the actual spot had been a narrow slit that spanned the width of the detector, it is possible that this electric field effect would have been observed.

We have not actually simulated moving the spot to an unaffected region of the detector after the first spot had been simulated. However, it is

27
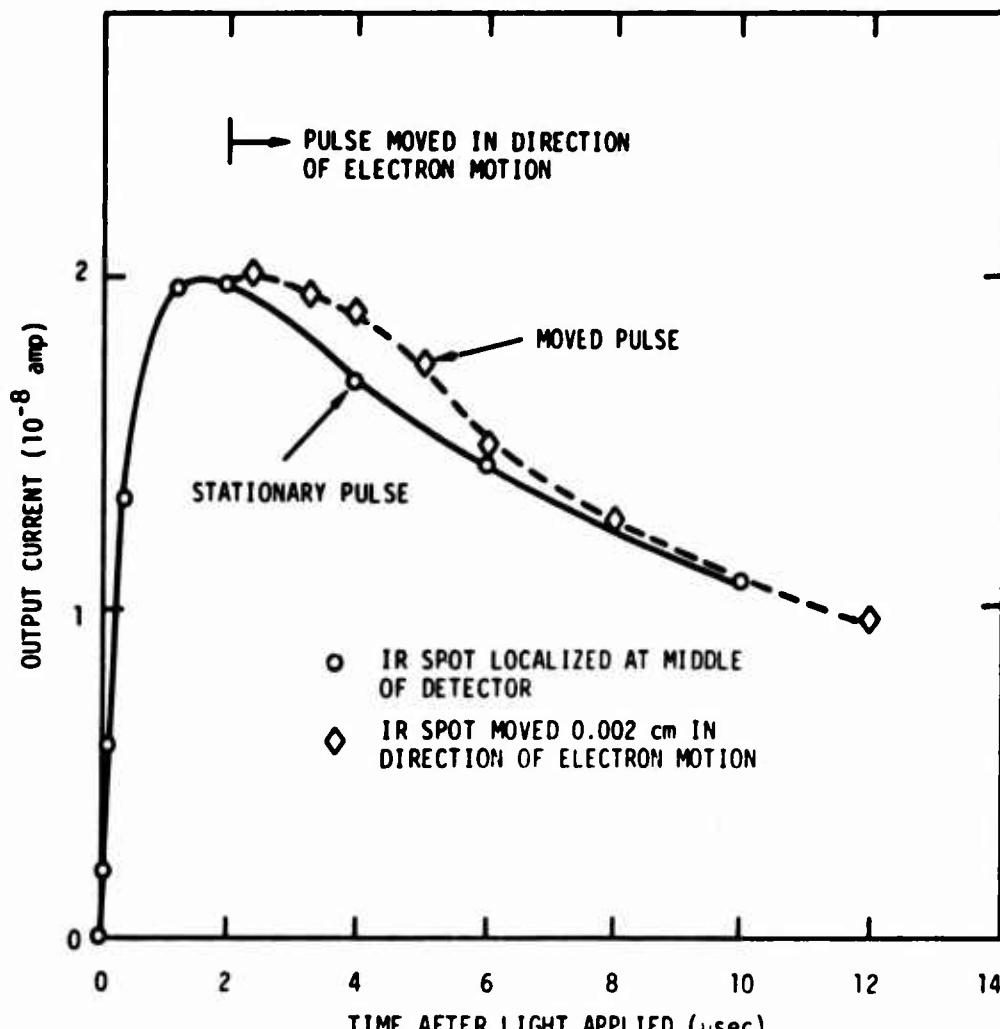
Figure 13. Time history of output current for a small stationary IR spot and with the spot moved to a new stationary location, low-field detector (5 V bias)

fairly evident that the response would repeat itself, starting from the initial low value, provided the second spot was not too close to the first. The following discussion illustrates what happens when the spot is moved to a new region but still within the region affected by the first spot.

At present, it is not practical to simulate a moving spot with the PN code. Therefore, to approximate this effect, it was decided to simulate a stationary spot for a certain length of time and then continue the problem with the spot moved only a short distance from its first location. This should roughly approximate the effect of a slowly moving spot. Due to the complication of the reduced local fields, which were discussed above, the time at which the change was made was chosen just after the first signal had reached a peak, but before the local fields had decreased too much. The resulting time history when the spot was moved in the direction of the drifting electrons is also shown in Figure 13. As expected, the signal shows an increase immediately after the spot is moved but then decays as the electric fields are reduced. The fact that the signal increases after the spot is moved indicates that the reduction in lifetime in the region covered by the new spot is more important than the reduction in electric field in this region.

Several predictions can be made from this model, and corresponding experiments could be performed to verify them.

1. The time for the signal due to a stationary spot to approach saturation should be inversely proportional to the intensity of the IR spot.

2. The time to saturation will probably increase with increased applied bias because the electrons will be trapped over a larger range than at low biases.

3. For a moving spot, the difference in signal for the two directions of motion should decrease with increasing sweep speed and increase with the intensity of the spot.

4. Both IR and bandgap background excitations should affect the magnitudes and time histories of the signals. However, there are several opposing effects due to excess carriers, and it is hard to estimate which will produce the dominant change.

29

2.3.3 Effect of Different Detector Properties and Operating Conditions

In this section we will analyze the effect of background illumination, applied field, detector thickness, and counterdoping on the response of the detector to a pulse of ionization. The results apply either to an IR pulse or across-the-gap excitation because, in the latter case, the minority carriers are quickly captured by the neutral-dopant atoms, which is equivalent to an IR excitation. The model for the low-field detector was again used with the PN code simulation to study these effects.

The effect of counterdoping density is shown in Figure 14. The density of ionized donors, which are the capture sites for free electrons, is roughly equal to the counterdoping in the one-trap model with a shallow acceptor trap that has a relatively small amount of trapped charge. Thus, the carrier lifetime and signal of the detector should be inversely proportional to the counterdoping in a non-sweep-out condition, according to the Shockley-Read formula. In Figure 14 this dependence is seen to be followed very well for small injection levels, $\Delta n \ll (N_D^+)_0$, where $(N_D^+)_0$ is the initial density of ionized donors — that is, essentially equal to the counterdoping density. However, the response becomes insensitive to counterdoping for large injection levels, $\Delta n \gg (N_D^+)_0$. In this case, the lifetime is determined primarily by the increase in N_D^+ caused by the ionization pulse. Figure 14 also indicates that the response time varies approximately inversely with the total density of ionized donors, $N_D^+ = (N_D^+)_0 + \Delta N_D^+$. These results are also given in Figure 15, which shows the deviation from the inverse linear behavior as the counterdoping is decreased. In fact, if the peak amplitudes are plotted versus the sum, $[(N_D^+)_0 + \Delta n]$, the result is fairly close to the curve for a linear variation.

Sweep-out effects at large fields are illustrated in Figure 16. These data are also shown in Figure 17 to illustrate the effect of the applied field on the peak signal. At fields of $\gtrsim 10^4$ V/cm, the transit time approaches the recombination time, $\sim 10^{-9}$ sec, so that the response becomes insensitive to the field. These results illustrate the effect of large variations in both applied bias and distance between the contacts.

Figure 18 shows the effect of varying the background illumination — i.e., the steady-state conductivity of the detector. It is seen that the
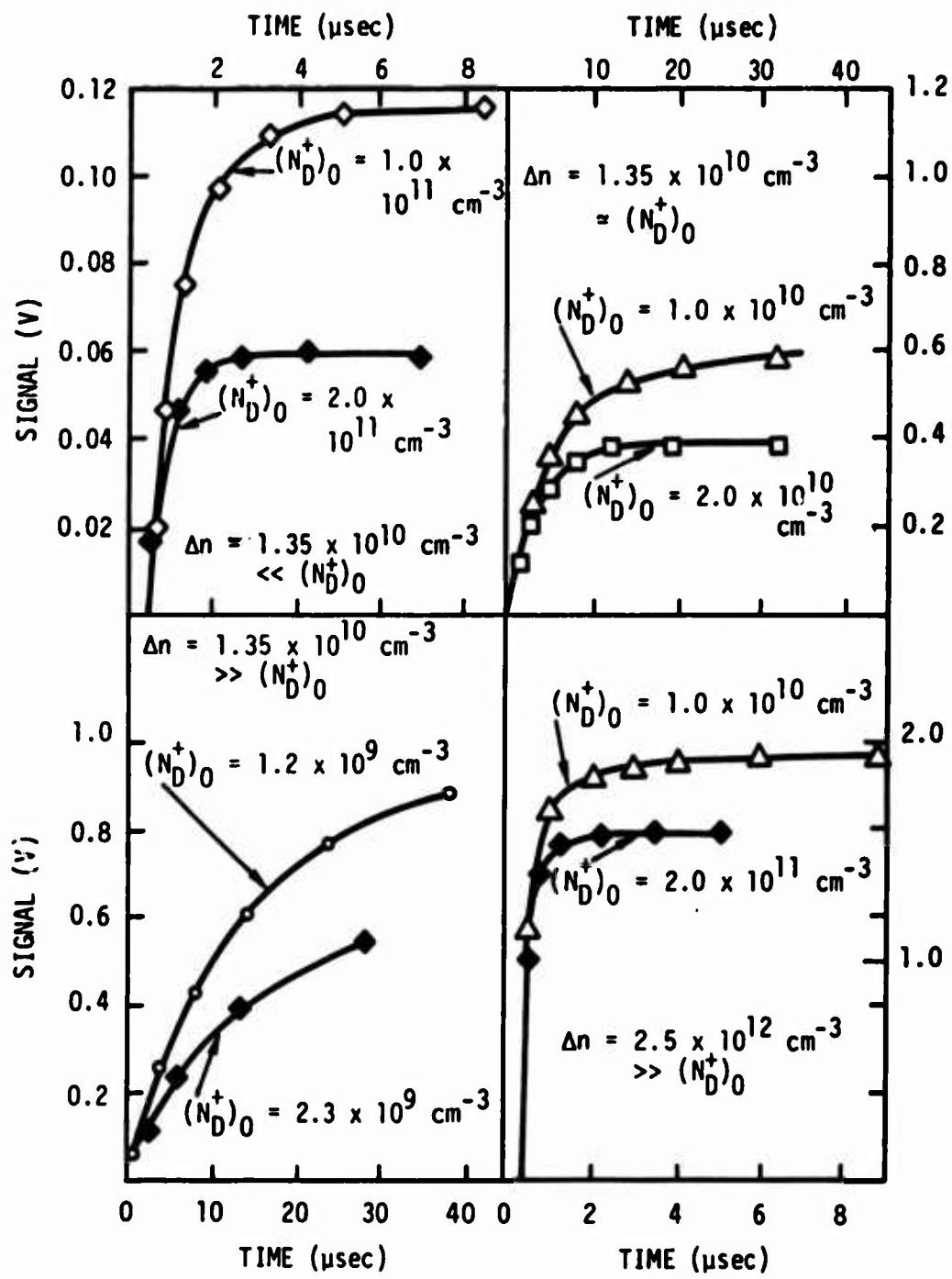
Figure 14. Effect of counterdoping, $(N_D^+)_0$, for large and small ionization levels, Δn
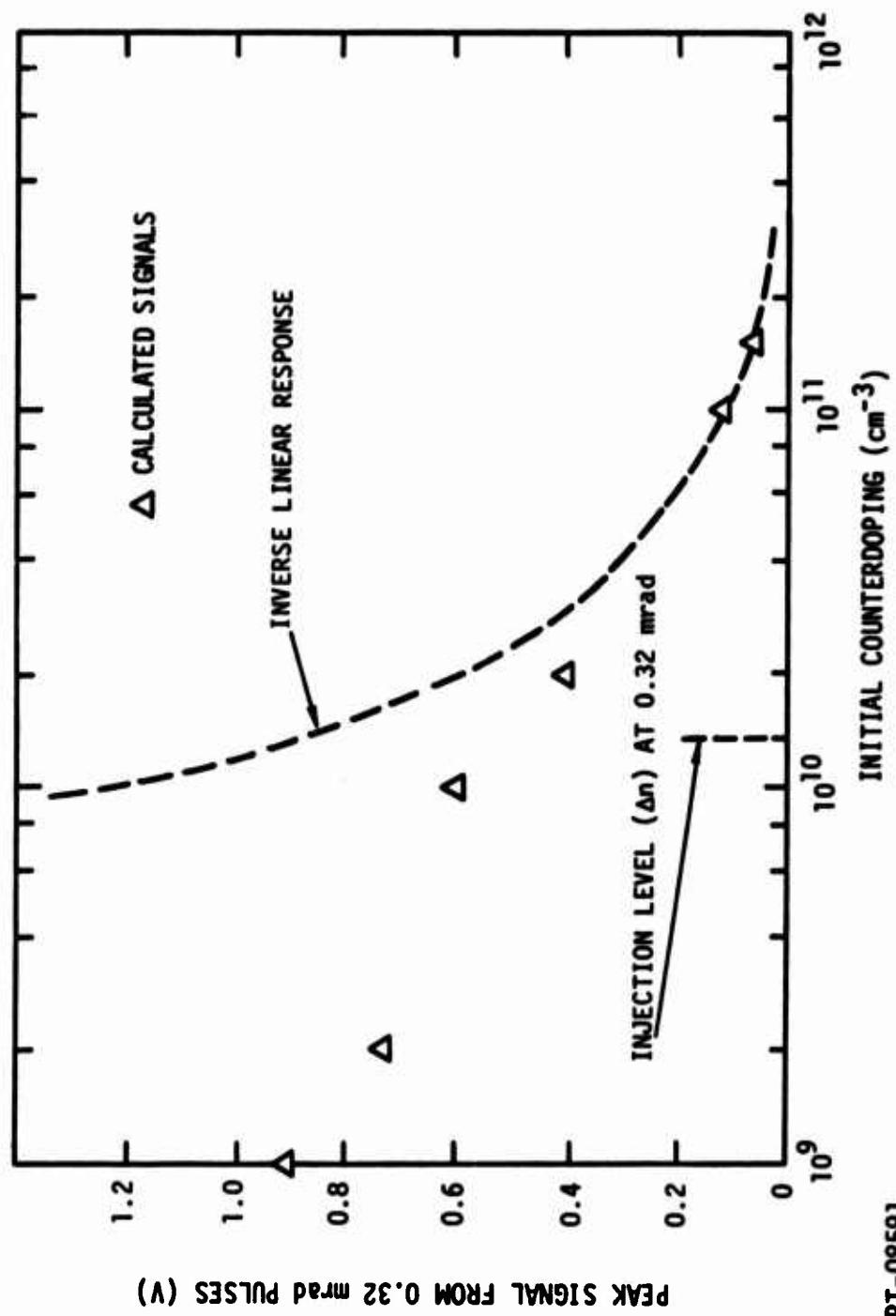
RT-08590

Figure 15. Effect of counterdoping on detector signal for constant injection level

RT-08591

32
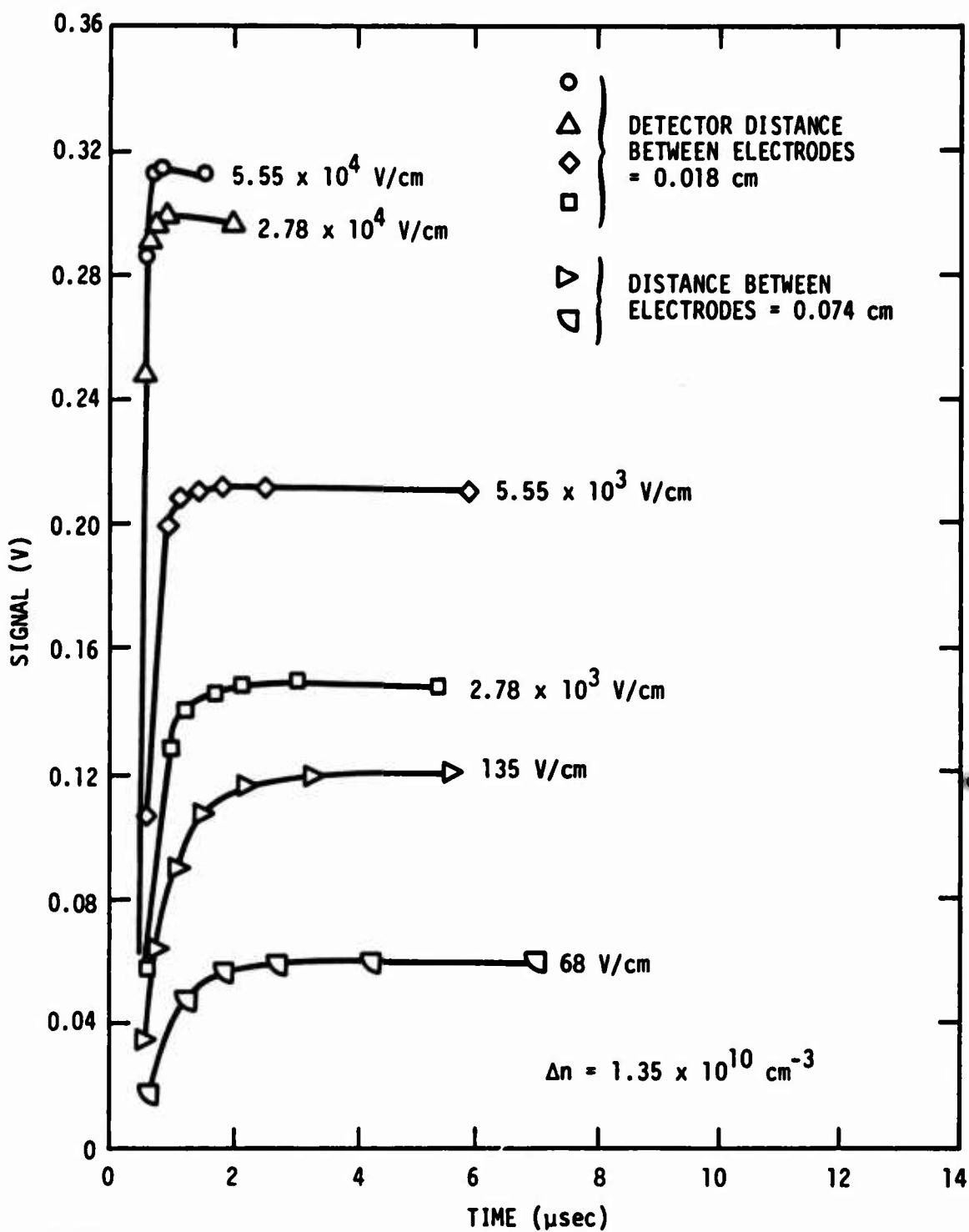
RT-08592

Figure 16. Field effect of detector response under sweep-out conditions

33
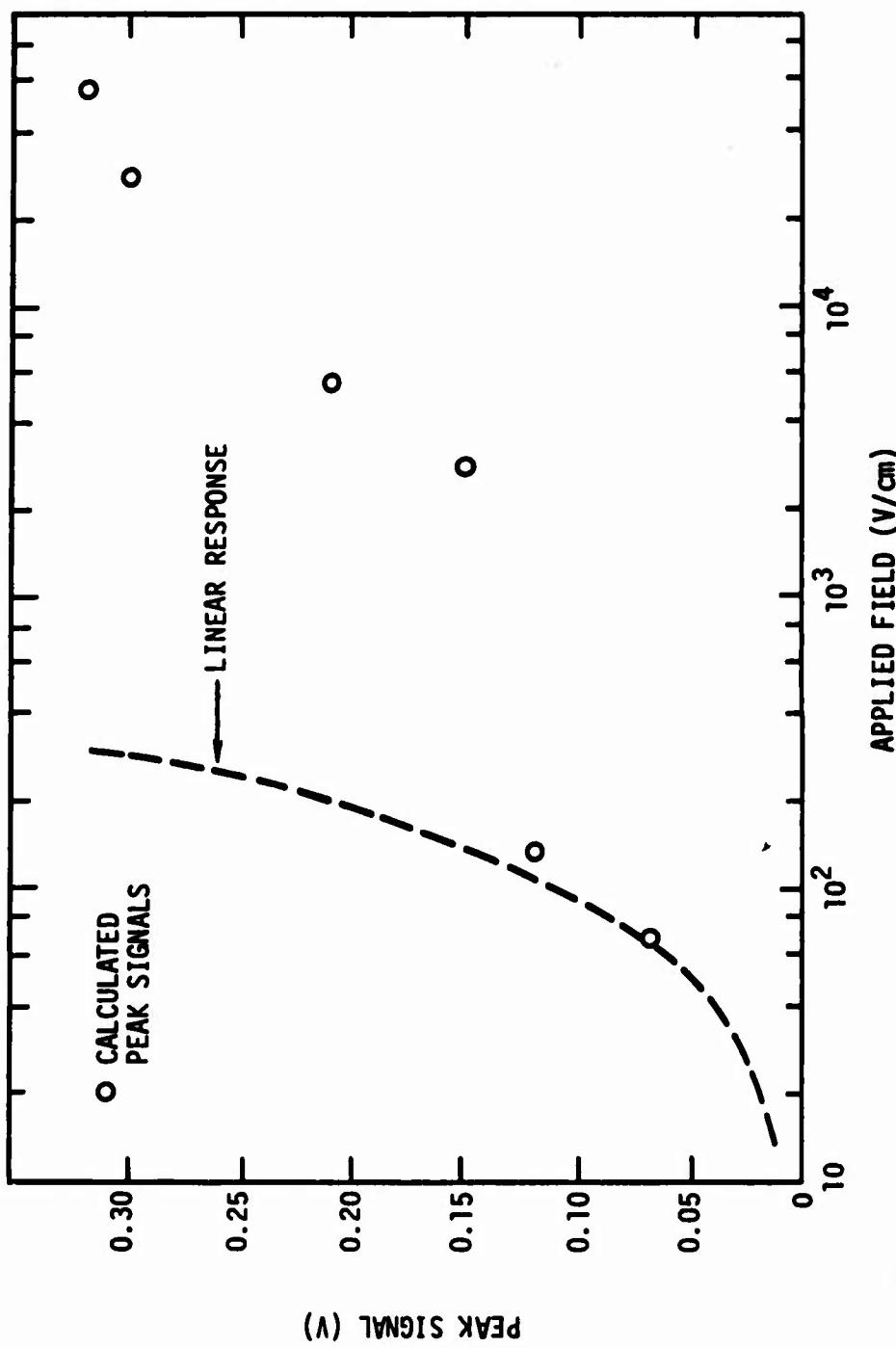
Figure 17. Effect of applied field on detector peak signal

RT-08593
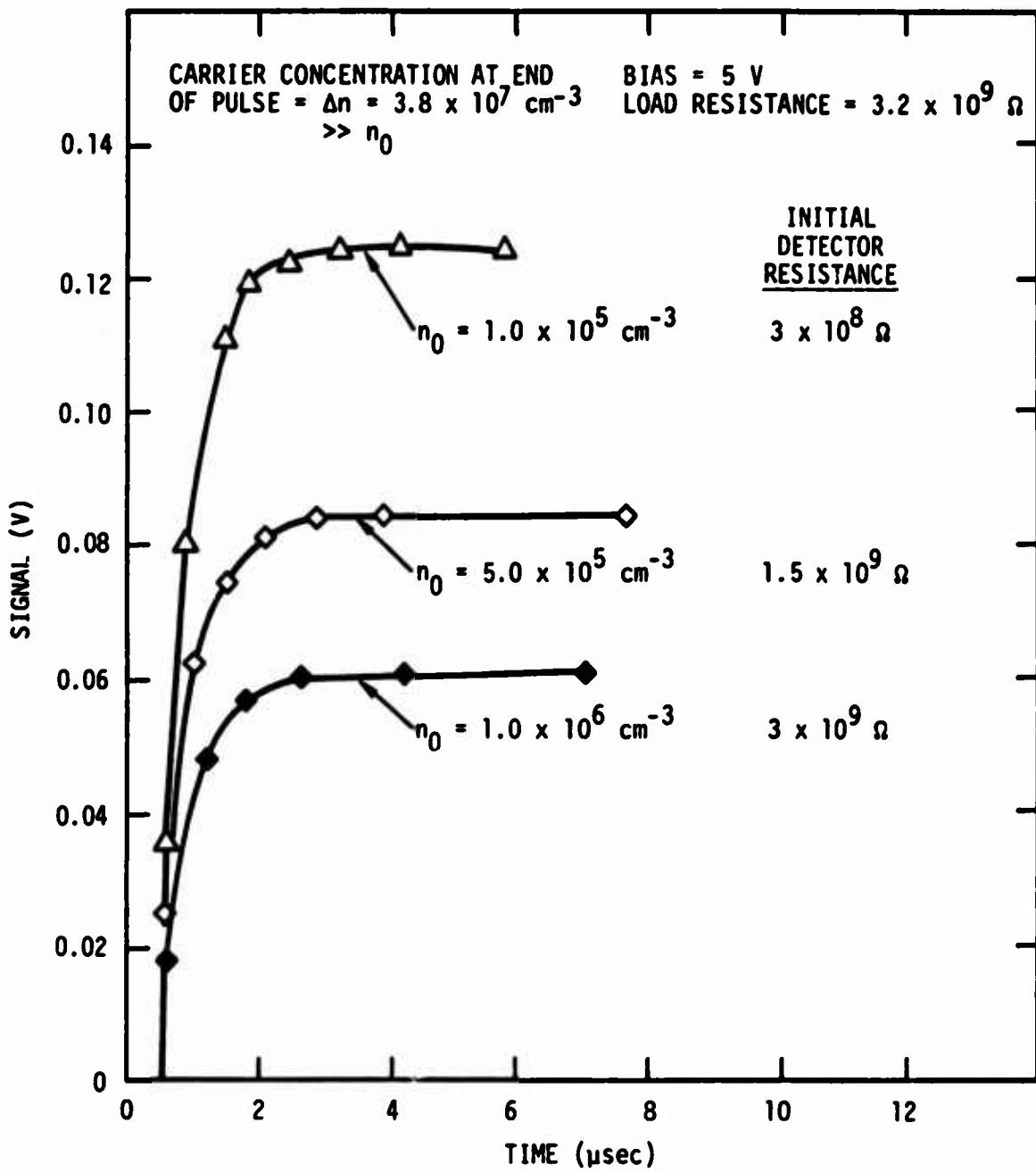
Figure 18. Effect of background illumination on detector response

RT-08594

signal increases as the background decreases n_0. This variation is due to the voltage saturation effect we observed in the Linac experiments (Section 2.2.2). For these simulations, the load resistance was comparable to the resistance of the detector with the largest n_0. Therefore, only about half of the applied bias appeared across the detector for this case, and the resulting signal was smaller than when the detector resistance was larger (n_0 less).

3. SPIKING

3.1 Introduction

Previous investigations of semiconductor infrared detector noise has revealed a characteristic "spiking" type of noise. This type of noise is easily discernable (under certain conditions) when viewed on an oscilloscope because it presents a very characteristic "spike" signature, as can be seen in the drawing of Figure 19.
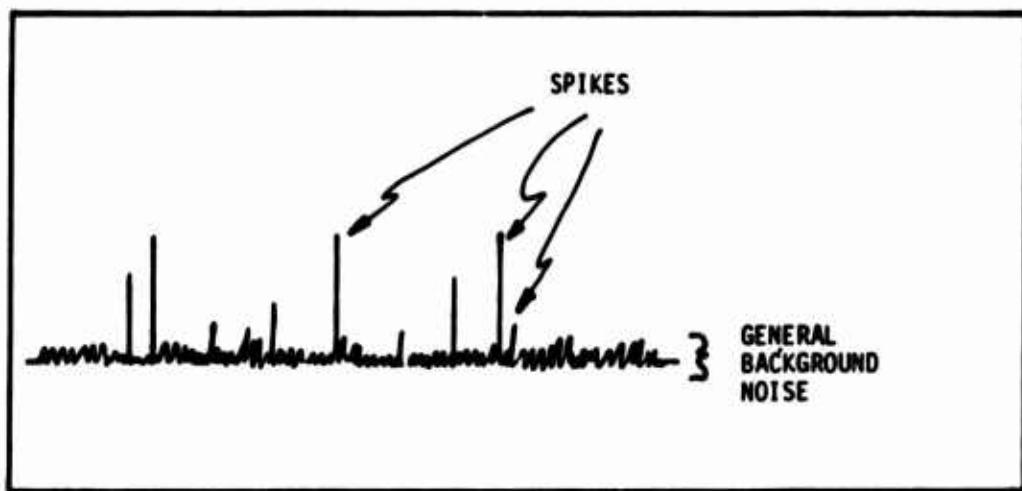
RT-07706

Figure 19. "Spike" noise oscilloscope representation

In general, this spike noise increases with (1) increasing detector bias and (2) increasing light irradiation. It has also been observed to start only after some time interval after light turn-on, generally from 10 to 100 msec.

The physical mechanism responsible for spiking noise is not known for sure, but it is thought to originate in the area of the contact to the detector material.

The purpose of this program is to experimentally investigate this spiking phenomenon with the hope of pinning down the physical mechanism responsible and to provide a basis for modeling the effect.

3.2 Experimental Description

3.2.1 General Block Diagram

A block diagram of the measurement circuit is presented in Figure 20. Light from the blackbody is mechanically chopped and passes through a cooled 2.7-μm filter to the sample. The resultant electrical signal is developed across a cooled load resistor (R_L), undergoes an impedance transformation in the cooled MOSFET, and then is measured in the PAR 124 lock-in amplifier. Bias for the detector is supplied by V_B through the load resistor, which has an impedance that is small compared to the detector impedance at 10°K. For a pulse-height analysis, the PAR 124 is replaced with a Technical Measurement Corp. CN1024 digital computer unit.

3.2.2 IR Detector Characteristics

The detector is a 1-mm cube of arsenic-doped (n-type) silicon which was fabricated at Rad Tech. Its room-temperature resistivity is 0.55 ohm-cm. Contact to the sample was made by gold foil alloyed at 450°C.

The detector figure of merit (D^*) was measured to be 1.1×10^{12} cm(Hz)$^{\frac{1}{2}}$/W at 2 volts bias, 20 Hz light chop, $\lambda = 2.7$ μm, $R_L = 2.15 \times 10^9$ ohms (at 300°K), and $T = 10°$K. Thus, this sample is a good-quality detector.

3.2.3 Time Constant Effects

The detector, load resistor, and distributed capacitance can be represented by the equivalent circuit of Figure 21. The value of C $(8 \times 10^{-12}$ farads) was determined by finding the $1/\varepsilon$ point for the detector signal when R_L was 3×10^7 ohms at 10°K.

To determine the true spike height and time duration, a low value of R_L is needed to keep the circuit RC small. This, however, causes a drop in signal amplitude as the ratio $R_L/(R_L + R_D)$ becomes smaller.

The smallest value of R_L that could be used was 10 kΩ (at 300°K), which was about 300 kΩ at 10°K. This gave a circuit response of $\tau = 2$ μsec.
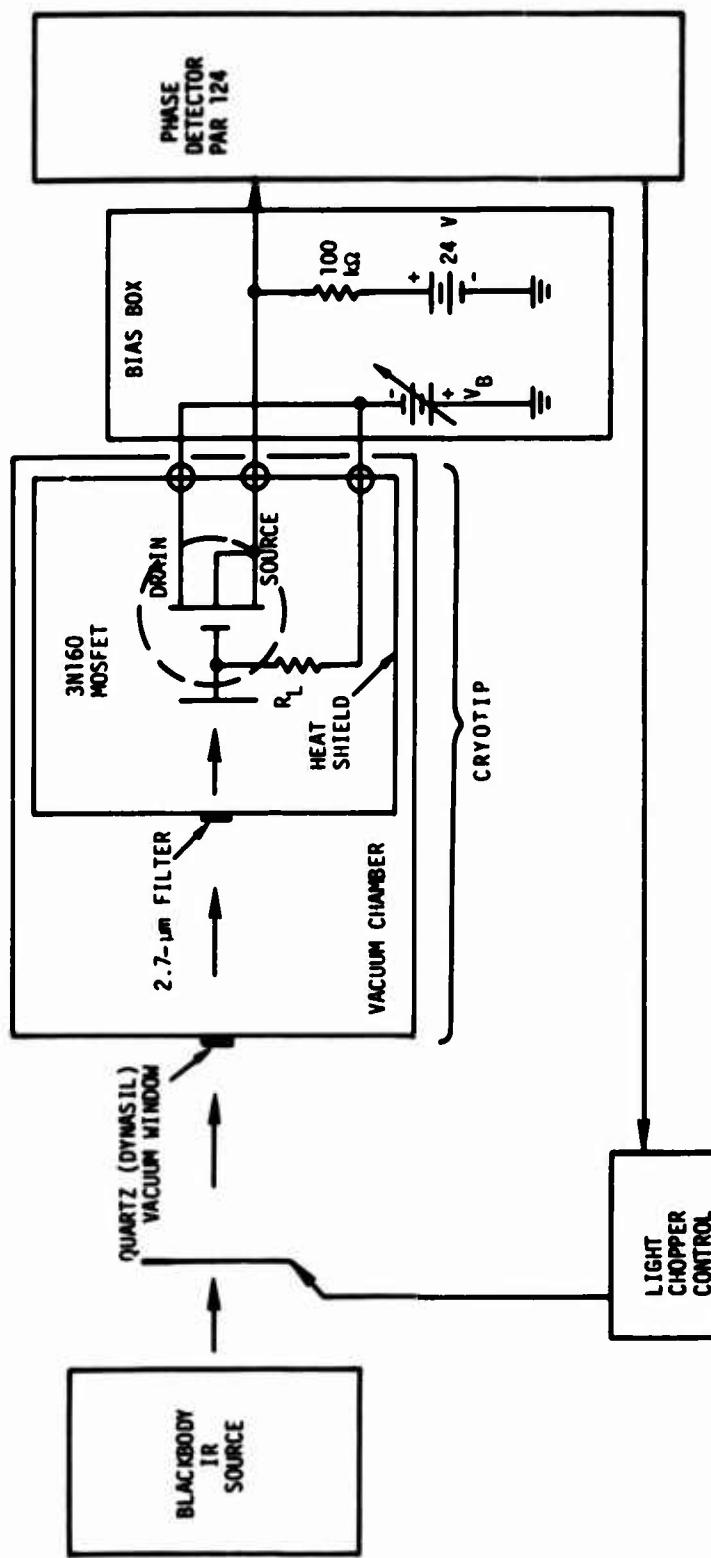
Figure 20. Block diagram of measurement circuit

RT-07715
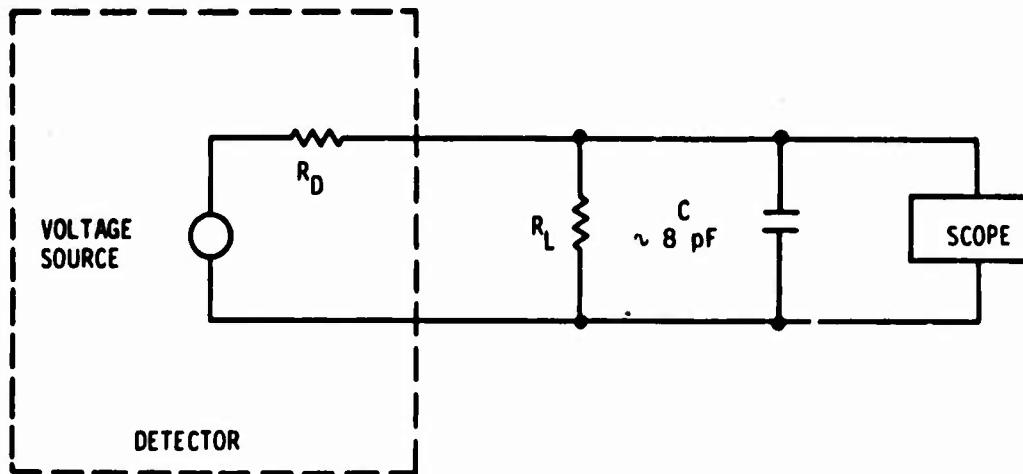
RT-07714

Figure 21.   Equivalent detector circuit

The optimum value of R_L, which gave a reasonable spike height, was 1 MΩ (at 300°K) or 30 MΩ (at 10°K). This gave a circuit response of τ = 200 μsec.

3.3   Discussion of Data

3.3.1   Bias Dependence

The noise level as a function of detector bias voltage for various illumination levels is presented in Figure 22. Spiking was evident when the noise level exceeded 10^{-5} volts. Note that in this region the rms (and peak-to-peak) noise levels vary approximately as the square of the bias voltage.

3.3.2   Illumination Dependence

The noise level as a function of sample illumination for two bias levels is presented in Figure 23. Note that the rms noise levels (and also the peak-to-peak spike heights) vary approximately as the square root of the sample illumination.

3.3.3   Time Delay Dependence

A rough dependence of the time delay for spiking as a function of illumination level is presented in Figure 24. The exact delay time is difficult

40
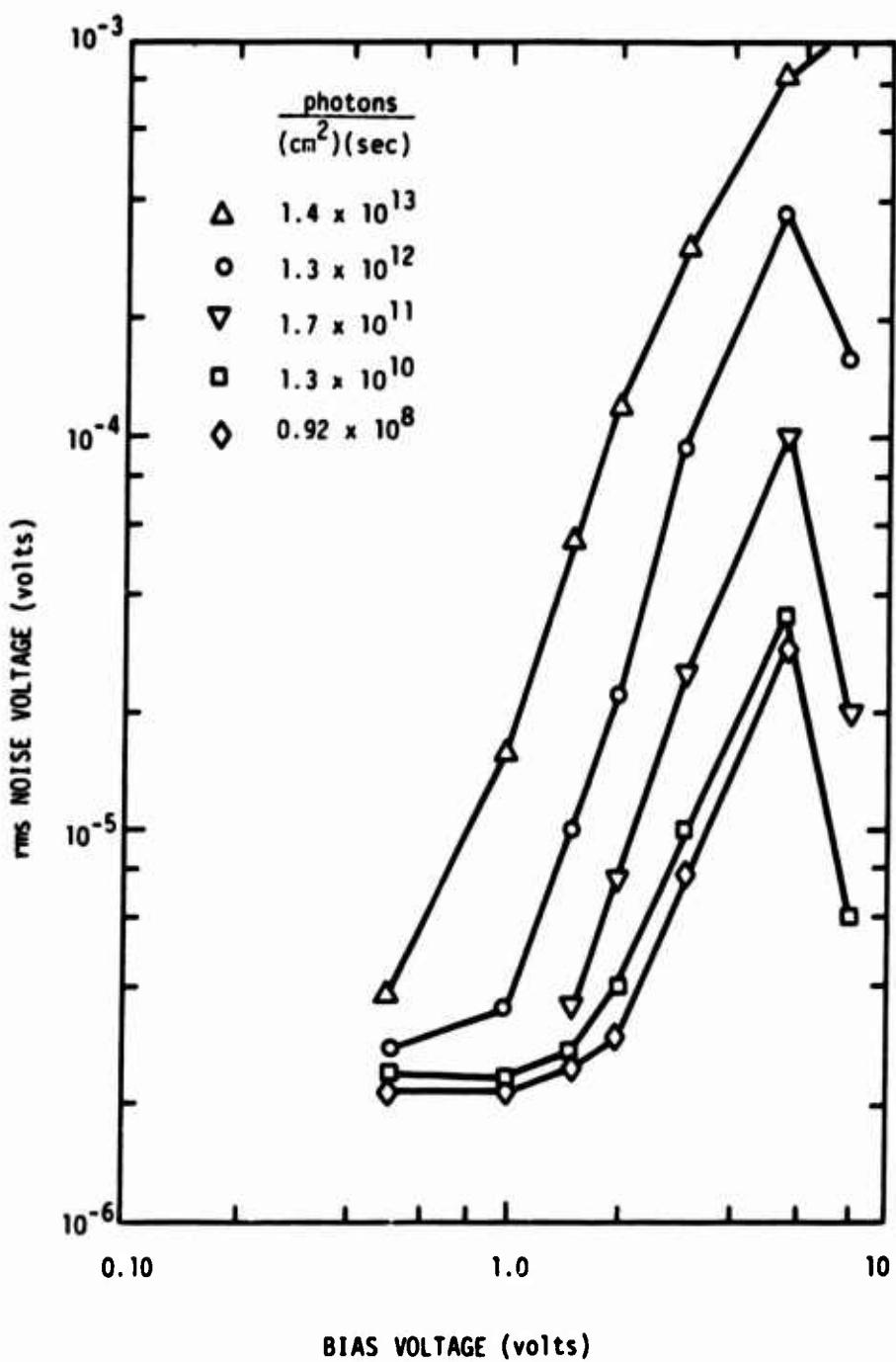
RT-07710

Figure 22. Noise versus bias as a function of background illumination

RT-07709
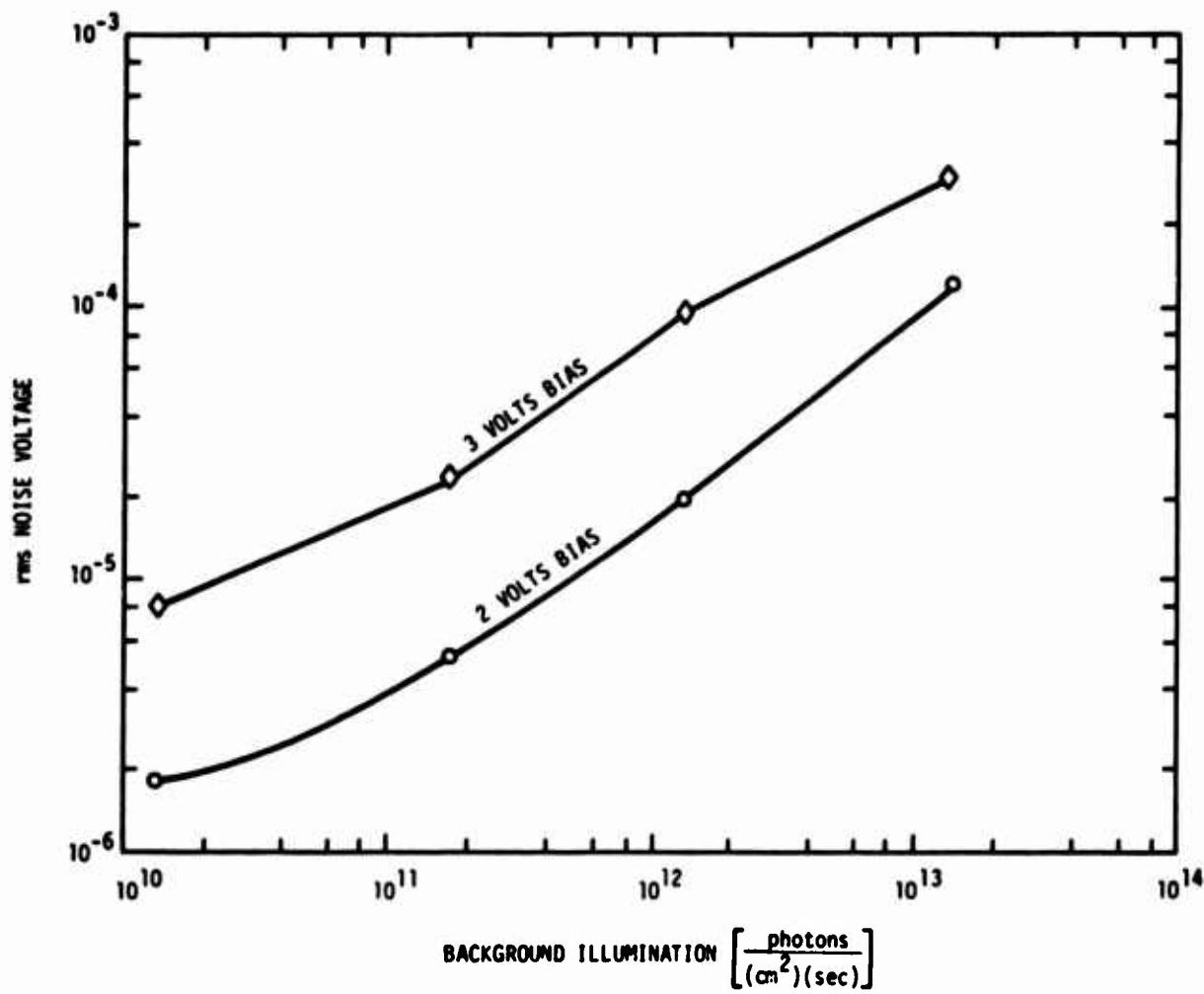
Figure 23. Noise versus background illumination as a function
of bias voltage

42
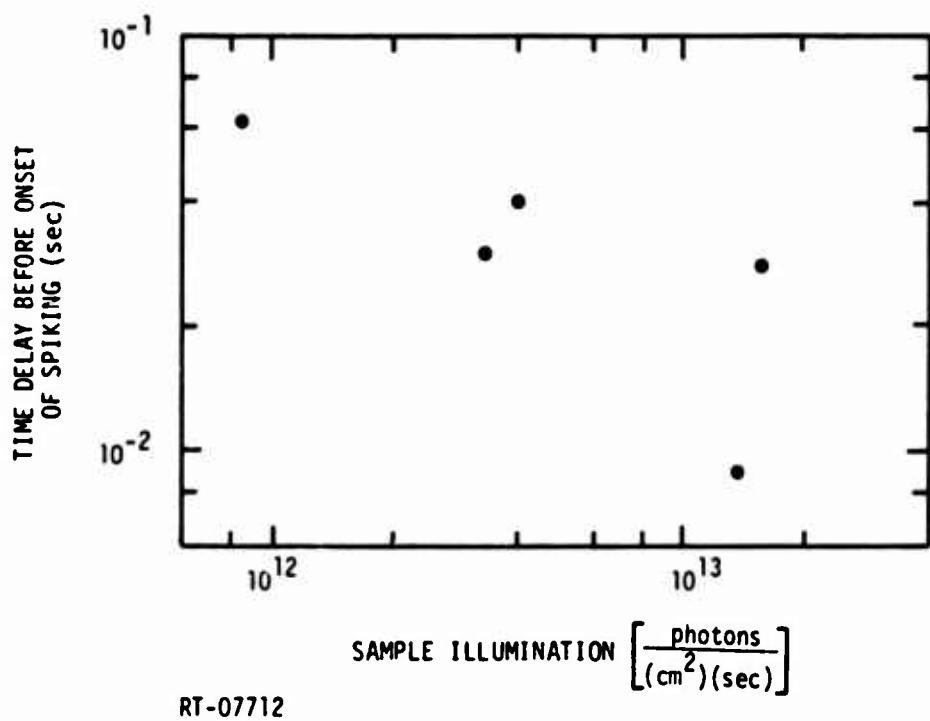
Figure 24. Time delay before onset of spiking after light-on
(5.5 V bias) versus sample illumination

to determine due to uncertainties in the light turn-on time, but the time of
the delay seems to vary inversely with the square root of the illumination
level.

A rough dependence of the time delay for spiking as a function of bias
is presented in Figure 25. For very small biases, there is no spiking so
the delay time approaches infinity at the threshold value.

Comparing these measurements with the previous data, it appears that
the time delay varies inversely with the spike amplitude. The larger the
spikes, the smaller the time delay.

3.3.4 Pulse-Height Distribution

An attempt was made to measure the number of spikes at a certain volt-
age level in a given unit of time to see if the distribution of these points
varied with bias or illumination level. No conclusive results were obtained,
but it appears that distribution has, at most, only a weak dependence on bias
and illumination.

Y-axis label: TIME DELAY BEFORE ONSET OF SPIKING (sec)

X-axis label: BIAS VOLTAGE (volts)
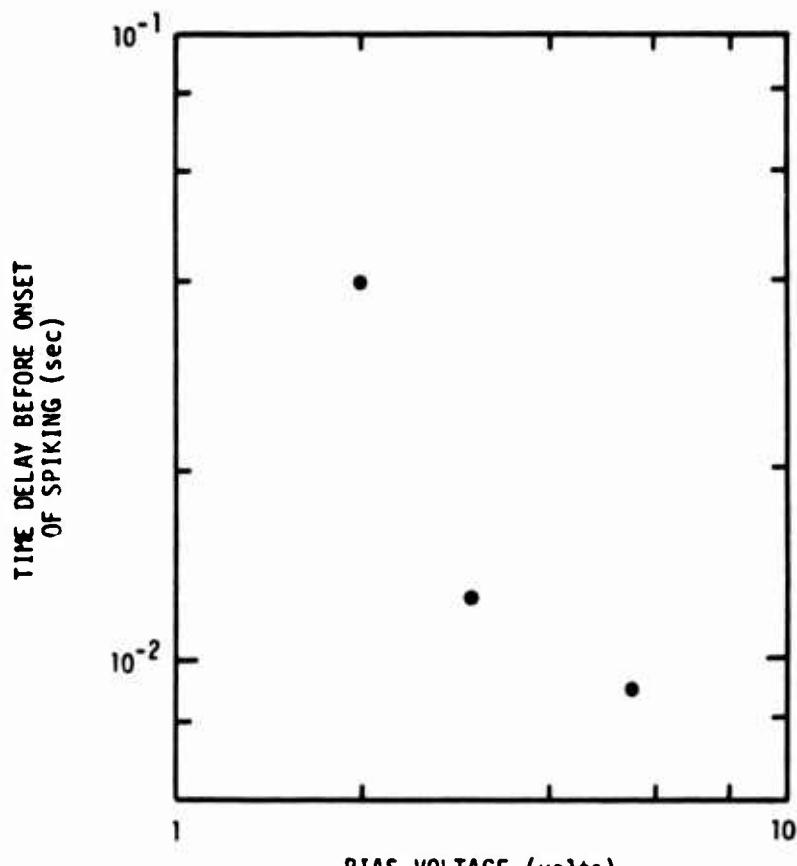
RT-07713

Figure 25. Time delay before onset of spiking after light-on
(9 x 10^{11} photons/cm^2-sec) versus bias voltage

3.3.5 Investigation of Spike Width

The load resistor was lowered to 10 kΩ (300°K) in an attempt to get the circuit time constant (τ) as low as possible, as was discussed in Section 3.2.3. The τ of this arrangement was about 2 μsec.

The spikes observed with this low value for R_L were still RC-limited; however, a tail was observed. Thus, a spike has a width less than ~1 μsec and may have a tail with a decay of a few microseconds.

Three interesting phenomena were observed with this low value of R_L which have not been found with the higher values of R_L:

　　　　1. Steady irradiation did not produce spikes; they were observed
　　　　　　only for a while after turning on the light.

44

2. The spikes disappeared about 1.4 sec after light-on, independent of light intensity.

3. Spikes disappeared 25 sec after bias was applied, independent of bias level.

It is interesting to note that if the spike disappearance is a direct function of load impedance, then the usual load resistance of 10^9 ohms would give a spike disappearing time of

$$(25 \text{ sec}) \left(\frac{10^9}{10^4}\right) = 2.5 \times 10^6 \text{ sec}$$

or 700 hours, which would never be seen in ordinary detector operation.

3.3.6 Time Between Spikes

For the 1-MΩ (at 300°K) load resistor ($\tau = 0.2$ msec) configuration, the smallest time interval between spikes was ~0.5 msec, with a 5.5-volt bias. The longest time between spikes was ~40 msec.

3.4 Summary of Data

1. Noise voltage amplitude varies with the square root of the illumination, and with the square of the bias.

2. The time delay for spiking onset varies roughly inversely with the square root of the illumination and inversely with the square of the bias. Thus, the time delay varies inversely with the amplitude of the spikes.

3. Spikes have a pulse width of less than 1 μsec and may have a small tail with a decay of a few microseconds.

4. A low value of R_L (10 kΩ at 300°K) produced three unusual effects:

    a. Spikes were observed only when light was turned on; steady irradiation did not produce it.

    b. Spiking disappeared after about 1.4 sec after light-on, independent of light intensity.

    c. Spiking disappeared 25 sec after bias applied independent of bias level.

5. For the 1-MΩ (at 300°K) load resistor ($\tau = 0.2$ msec), the smallest time interval between spikes was about 0.5 msec.

3.5 Tentative Model

The following is a tentative model for the observed spiking phenomenon. This model will be tested later on the PN code.

Assume that contacts to the detector are partially blocking for electrons (or holes) to enter the semiconductor due to the potential barrier from the metal Fermi level to the semiconductor conduction (or valence) band. On the other hand, the electrons and holes in the semiconductor that reach the interface can freely enter the metal contacts. The term "partially blocking" is intended to mean the following. The thermalization time for excited electrons in the metal is assumed to be very short. Therefore, the electrons in the metal will always be essentially in thermal equilibrium, even when the metal is illuminated. Thus, the energy distribution of electrons in the metal is described by the equilibrium Fermi function centered on the metal Fermi level. Only those electrons with energies above the conduction band edge at the metal-semiconductor interface can be drawn into the semiconductor conduction band by an electric field. In thermal equilibrium, the electrons in the semiconductor conduction band are described by the same Fermi function as in the metal, and the electrons are continually crossing the interface in both directions, giving a zero net current. If a small bias is applied to the detector *in the dark*, the electrons that are swept away from the interface into the semiconductor are replaced by an equal number of electrons from the metal. A steady electrical current can flow and the contact is non-blocking. Now, if the device is suddenly illuminated, the density of electrons in the semiconductor conduction band will start to increase, and a larger current will try to flow in the semiconductor for the same applied field. However, the density of electrons that can enter the conduction band from the metal is the same as without illumination, because the metal is assumed to remain in thermal equilibrium. Therefore, the current from the metal to the semiconductor is less than the current that would like to flow in the semiconductor, and thus the contact is partially blocking.

Physically, what happens when the above situation arises is that electrons are swept away from the interface toward the interior of the semiconductor, and a net positive charge, due to holes and ionized donors, is left behind in the semiconductor near the interface. This positive charge causes

46

the electric field at the interface to increase until enough electrons can be pulled from the metal into the semiconductor to just replace those that are swept away toward the interior of the semiconductor. A new steady-state current, corresponding to the particular illumination intensity and bias, is then established. The magnitude of the steady-state field at the interface increases with bias and illumination. This steady-state condition is not established instantaneously because usually additional donor atoms have to be ionized to create the required electric field. This ionization can be either thermally or optically activated, but both processes can take a significant amount of time.

It is postulated that the spiking occurs when the electric field at the interface reaches a critical level and the barrier momentarily breaks down due to avalanching, tunneling, or some other process, producing a spike of current. This explanation is consistent with the observed facts that the spiking does not occur until some time after the illumination is turned on, the spiking is worse for heavy illuminations, and there is a bias threshold below which spiking is not observed. Under steady-state bias and illumination, the high field region near the interface may become very narrow. In this condition, tunneling would occur easily and smoothly and the width of the high field region may be too narrow for a significant avalanche generation to occur. This could explain why spiking apparently does not occur under steady-state conditions with a small RC. At present, it is not known whether avalanching is the mechanism by which the spiking occurs. Different mechanisms will be simulated on the PN code to see if the characteristics of the spiking phenomena can be reproduced.

4. PHOTOVOLTAIC DETECTORS

Much of the work that has been done on modeling silicon photoconductive detectors is also useful for developing a model for silicon photovoltaic detectors. However, the latter have several additional features, such as the built-in field in the junction, which strongly influences their response to radiation inputs. Thus, to correctly model such devices, it is necessary to have a reasonable estimate of the detector characteristics, such as its doping profile, recombination lifetime (diffusion length), built-in potential, etc. The doping profile and built-in potential can be estimated from capacitance-voltage measurements. For some devices, the diffusion length can be obtained from the short-circuit current when the device is illuminated with penetrating light so that the ionization rate is essentially uniform throughout the volume of the device. In other detectors which have wide depletion widths relative to the cell thickness, a better estimate of the lifetime can be obtained from the decay of the short-circuit current after a pulse of ionization. In addition, as a check on the correctness of the simulation, it is convenient to have the diode I-V curve, the detector responsivity as a function of wavelength and reverse bias, and the relative response under reverse bias to penetrating light (light filtered through silicon).

For our first attempt to obtain data on photovoltaic devices in preparation for modeling them, three commercial silicon photovoltaic detectors were purchased from Electro Nuclear Laboratories (PVS 020). Silicon was chosen as the material for these first photovoltaic studies to take advantage of the vast amount of information on silicon and to utilize, as much as possible, the results of our previous photoconductive modeling work. At a later date, it is hoped to extend this modeling work to other photovoltaic semiconductor materials. The specific devices were selected from a list of several typical detectors, primarily on the basis of cost. Although these detectors have been suitable for these first exploratory

48

experiments, the results indicate that it might be desirable to perform any additional work on better-quality devices for which the specifications are better known. This subject is discussed again later. For these devices, capacitance-voltage measurements have been made along with RMS and dc detector responsivity, short-circuit current, and the dependence of the response on reverse bias.

4.1 Description of Devices

Table 2 summarizes the known information on the photovoltaic detectors used thus far in this program. The quoted lifetimes are the values for the bulk material before the detector fabrication process was begun. It is not known for sure how these lifetimes may have been altered by the fabrication process.

TABLE 2. SPECIFICATIONS FOR PHOTOVOLTAIC DETECTORS

Manufacturer	Electro Nuclear Laboratories
Model Number	PVS 020
Base Material	p-type silicon
Dopant	Boron
Resistivity, ρ	350 ohm-cm
Lifetime, τ	200-350 μsec
Thickness	0.025-0.029 cm
Junction	
Type	Diffused
Dopant	Donor not known
Structure	Mesa, 2 mm square
Contact	Sputtered gold

4.2 Detector Responsivity

For purposes of this program, the responsivity is defined as the current produced by the detector operating in the short-circuit condition per unit incident radiant power.

Two methods were used to measure the current and will be referred to as the rms responsivity and the dc responsivity, respectively.

Measurements of the rms responsivity were made using the experimental arrangement shown in Figure 26a. Light from a tungsten filament was filtered using several narrow-passband interference filters covering the desired wavelength region (typical bandwidth of each filter was ∿0.010 μm) and mechanically chopped to produce a modulated irradiance with a known rms value. Power to the lamp was provided by a regulated power supply. Calibration of the system was performed using a Hewlett-Packard model 8330A radiant flux meter placed in the detector position to measure the steady-state monochromatic radiation. The equivalent rms radiant power is then

$$H_{rms} = 2.22 \, H_0$$

where H_0 is the steady-state radiant power and the coefficient is a correction factor related to the chopping efficiency.

The rms responsivity is then

$$R_{rms} = \left(\frac{1}{2.22 \, H_0}\right)\left(\frac{V_{rms}}{rA}\right)$$

where V_{rms} is the voltage across the detector (or the load resistance) operated near the short-circuit condition, r is the low-value load resistor, and A is the active area of the detector. The detector was operated in approximately the short-circuit condition by using a low-value load resistor, typically 100 ohms. This value was chosen by plotting the detector current against the voltage for several load resistances and choosing the smallest value to yield an adequate signal near the short-circuit condition. Bias was applied to the detector by a well by-passed variable-voltage power supply.

The dc responsivity is given by

$$R_{dc} = \frac{I_{dc}}{H_0 A}$$

where I_{dc} is the value of the current resulting from the incident radiation, extrapolated to zero voltage. Figure 26b shows the experimental arrangement used to measure the dc responsivity as a function of wavelength.

50
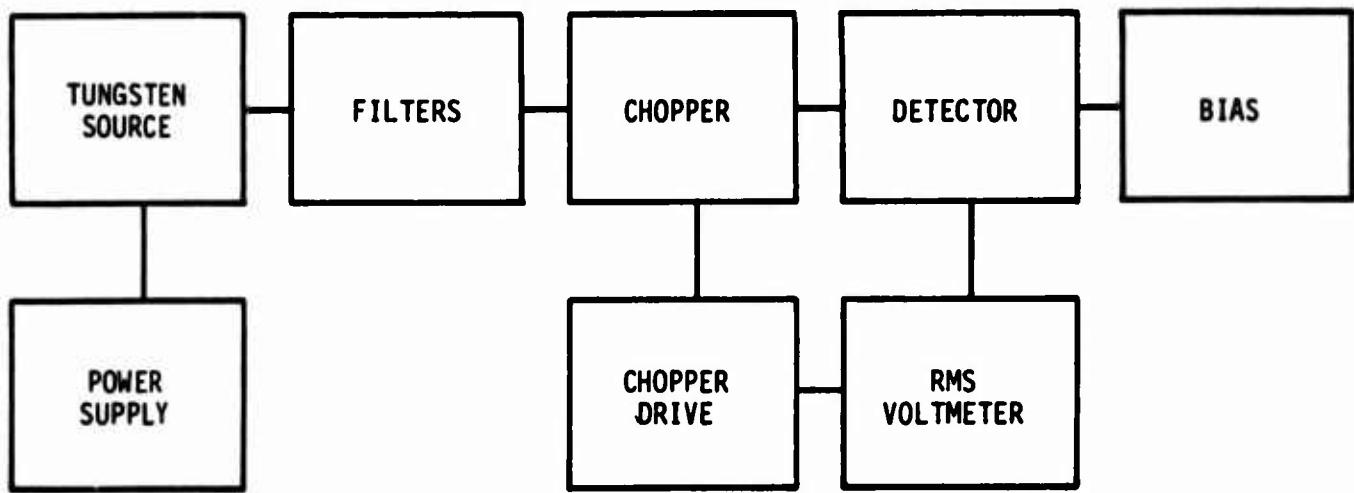
Figure 26a. Schematic of the experimental arrangements used to measure the rms responsivity
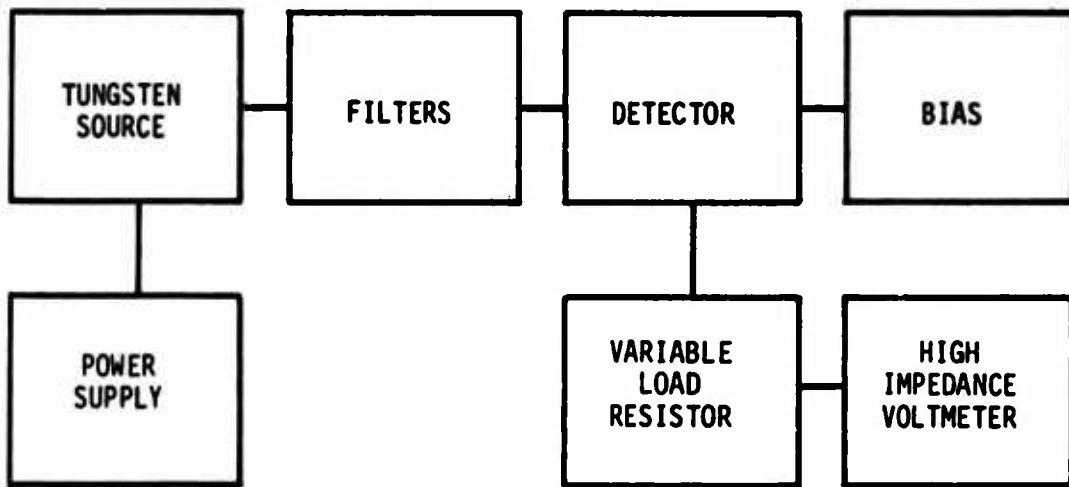

RT-08595

Figure 26b. Schematic of the experimental arrangement used to measure the dc responsivity and diffusion length

Figure 27 shows the rms responsivity as a function of wavelength for the three photodetectors. Detectors 2 and 3 were measured without their protective glass caps and should have yielded a slightly higher responsivity than detector 1 with its cap in place. Although detector 3 does show this small enhancement, detector 2 does not. Other measurements show detector 3 to be unstable, perhaps due to adsorbed contaminants on the wafer. The measured rms responsivity is slightly higher than the minimum quoted by the manufactures, but, although not unreasonably small, it does not compare to the dc responsivity measured by the steady-state technique.

The dc responsivity of detector 1 was determined at four wavelengths by measuring the short-circuit current under a steady-state irradiance; these data are shown in Figure 27 (□ data points) along with the rms responsivities.

Figure 28 shows a typical dc I-V curve of the steady-state current versus the voltage across the detector under a known steady irradiance, with the load resistor as the variable. As the load resistor is reduced to zero, the current goes to the short-circuit current. This value of current gives a responsivity of 0.57 amp/W at 0.902 μm, which is in good agreement with the specifications. The discrepancy in the two responsivities calculated for the same detector apparently is due to the difficulty in comparing a steady-state measurement to an rms measurement made by a mechanically modulated irradiance.

The application of a reverse bias enhances the responsivity by increasing the size of the depletion volume and by decreasing the carrier sweep-out time. Because the applied bias has little effect on the collection efficiency of the thin region between the front surface and the junction, the enhancement is expected to be small or nonexistent at short wavelengths and pronounced at longer, more penetrating wavelengths. The effect of an applied reverse bias is shown in Figure 29. The curve does, however, show a slight enhancement of responsivity due to bias at the shortest wavelength; while the manufacturer's specifications also show a slight enhancement, it is much larger than expected. The effect can be due to a spectral shift toward the shorter wavelengths resulting from a higher source temperature caused by small variations in the power level.
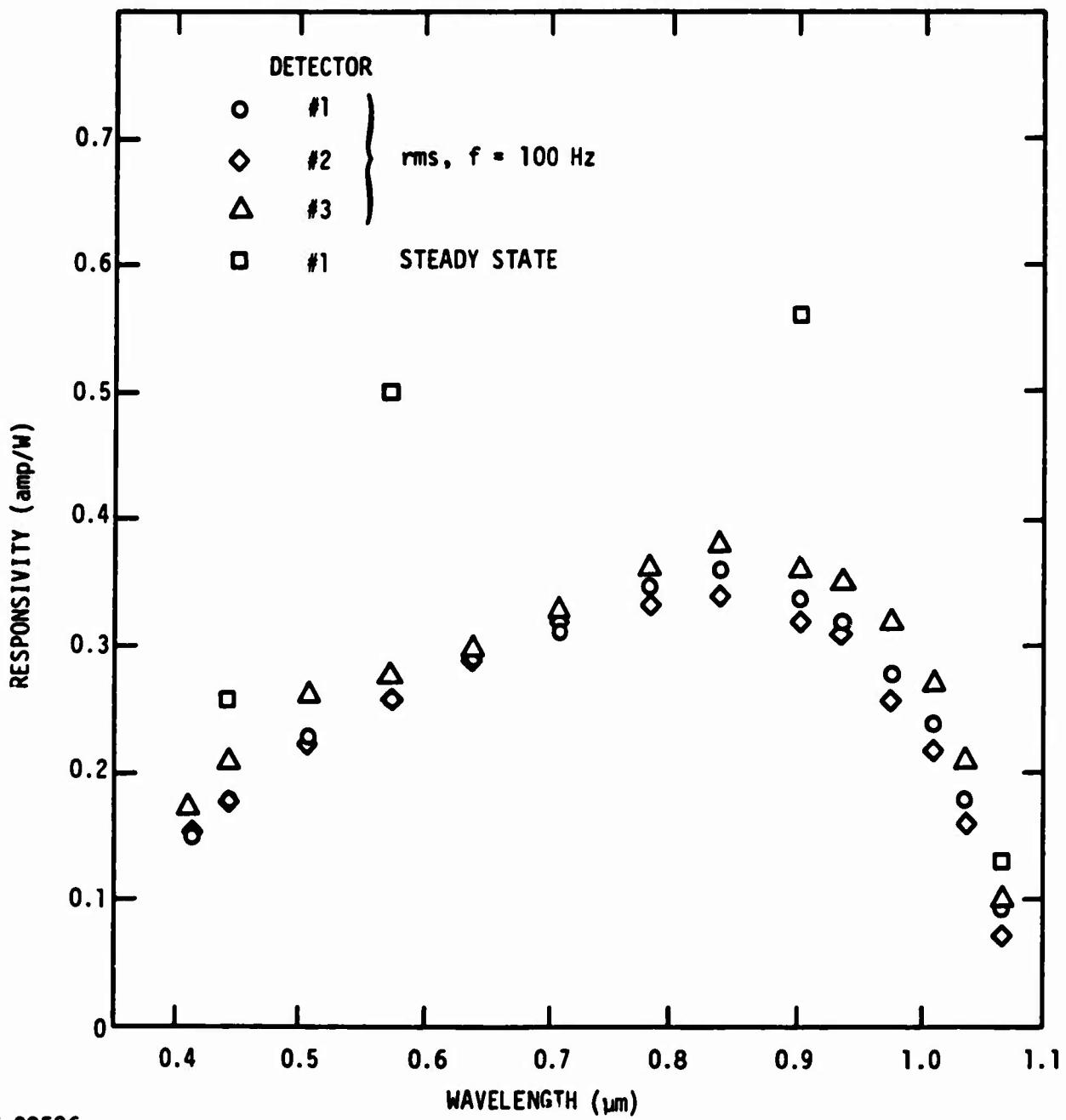
Figure 27. Responsivity as a function of wavelength for three detectors;
$V_{BIAS} = 0$

RT-08597
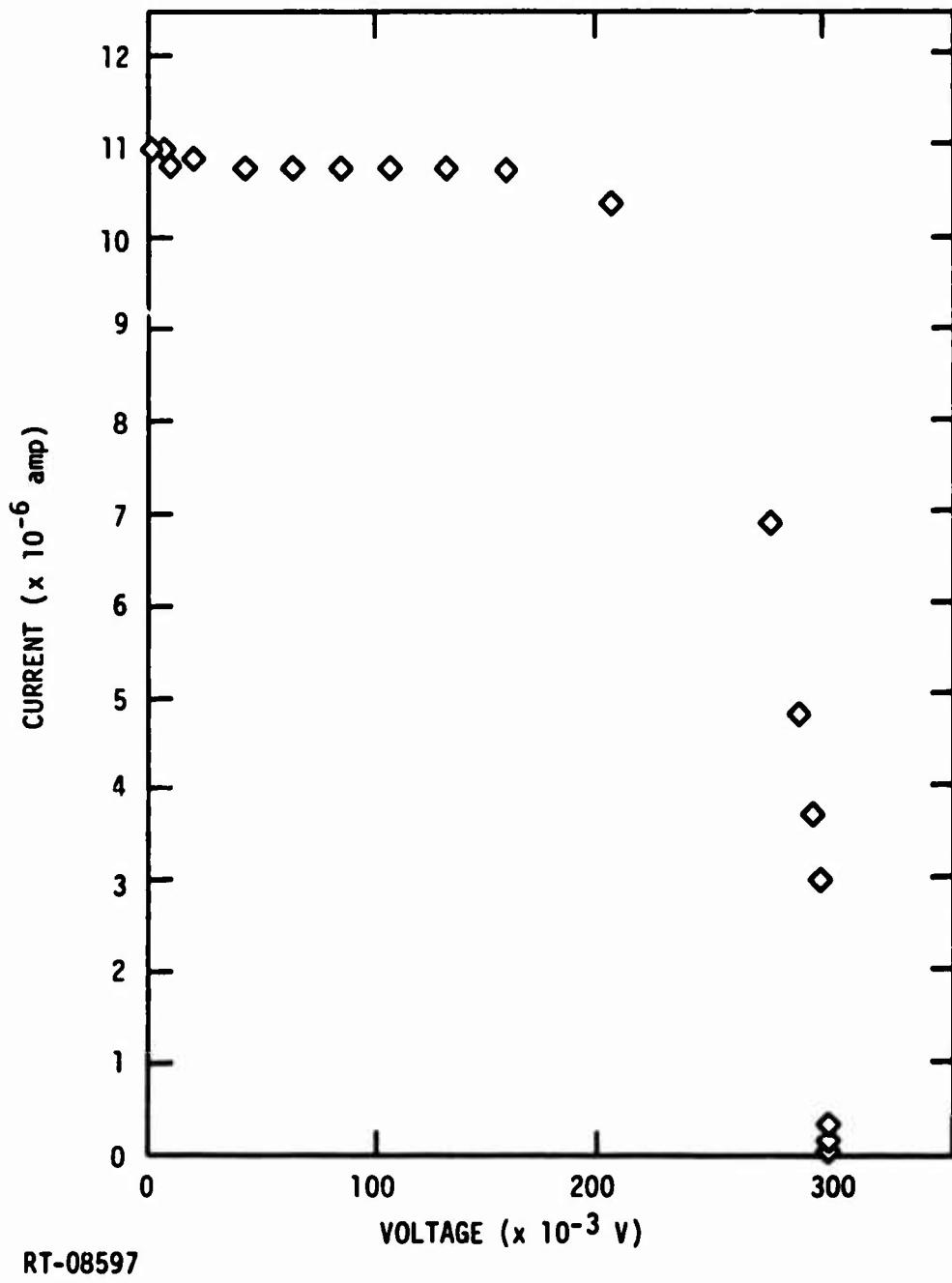
Figure 28. Typical current versus voltage plot used to determine the short-circuit current and open-circuit voltage (detector 1; wavelength = 0.902 µm)

54
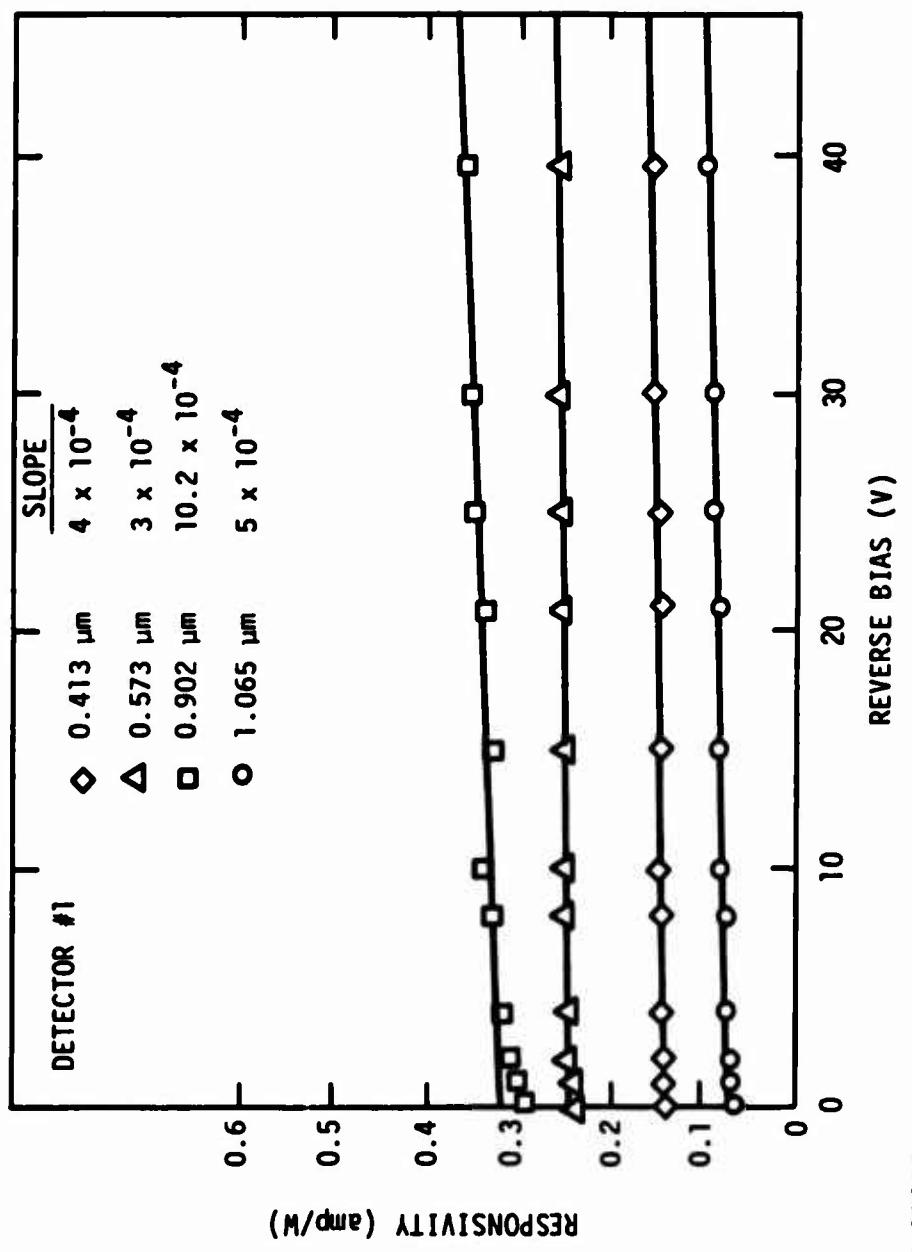
Figure 29. Responsivity as a function of reverse bias at several wavelengths (detector 1, f = 100 Hz)

RT-08626

4.3 Diffusion Length

The short-circuit current for a photovoltaic device can be written as

$$I_{SC} = q \, AG \, (L_f + W + L_b)$$

where q is the electronic charge, A is the illuminated area, G is the ionization rate due to the light source and is assumed to be uniform over the active volume of the device, L_f is the minority-carrier diffusion length or thickness (whichever is less) of the front surface region, W is the junction depletion width, and L_b is the minority-carrier diffusion length or thickness (whichever is less) of the base region. For solar cells with thin front regions, abrupt junctions, and long lifetimes in the base, $(L_f + W)$ is negligible compared to L_b, and the base diffusion length can be obtained from the short-circuit current by the equation

$$L_b = \frac{I_{SC}}{q \, AG} \quad ,$$

provided the base width is greater than L_b. Based on the manufacturer's quoted lifetimes (Table 2), it was assumed that L_b would be large compared to $(L_f + W)$. Therefore, I_{SC} was measured as a function of calibrated generation rates G and the base diffusion lengths were calculated by the above formula.

The light source used was a tungsten filament lamp with a water-cooled silicon filter to remove all wavelengths shorter than the silicon absorption edge. Since the wavelengths that get through the silicon filter are only weakly absorbed in the silicon detector, the generation rate G should be reasonably uniform throughout the detector. The equivalent generation rate of the source at the detector position was determined by using a calibrated solar cell whose diffusion length was accurately known. For a more uniform ionization rate throughout the volume, a more penetrating radiation, such as gamma rays, could be used but the present technique is considered adequate for now.

Figure 30 shows the base diffusion lengths for three detectors, calculated by the above method, as a function of the generation rate. Using an average value of $L_b = 0.02$ cm from Figure 30 and a minority-carrier (electron)
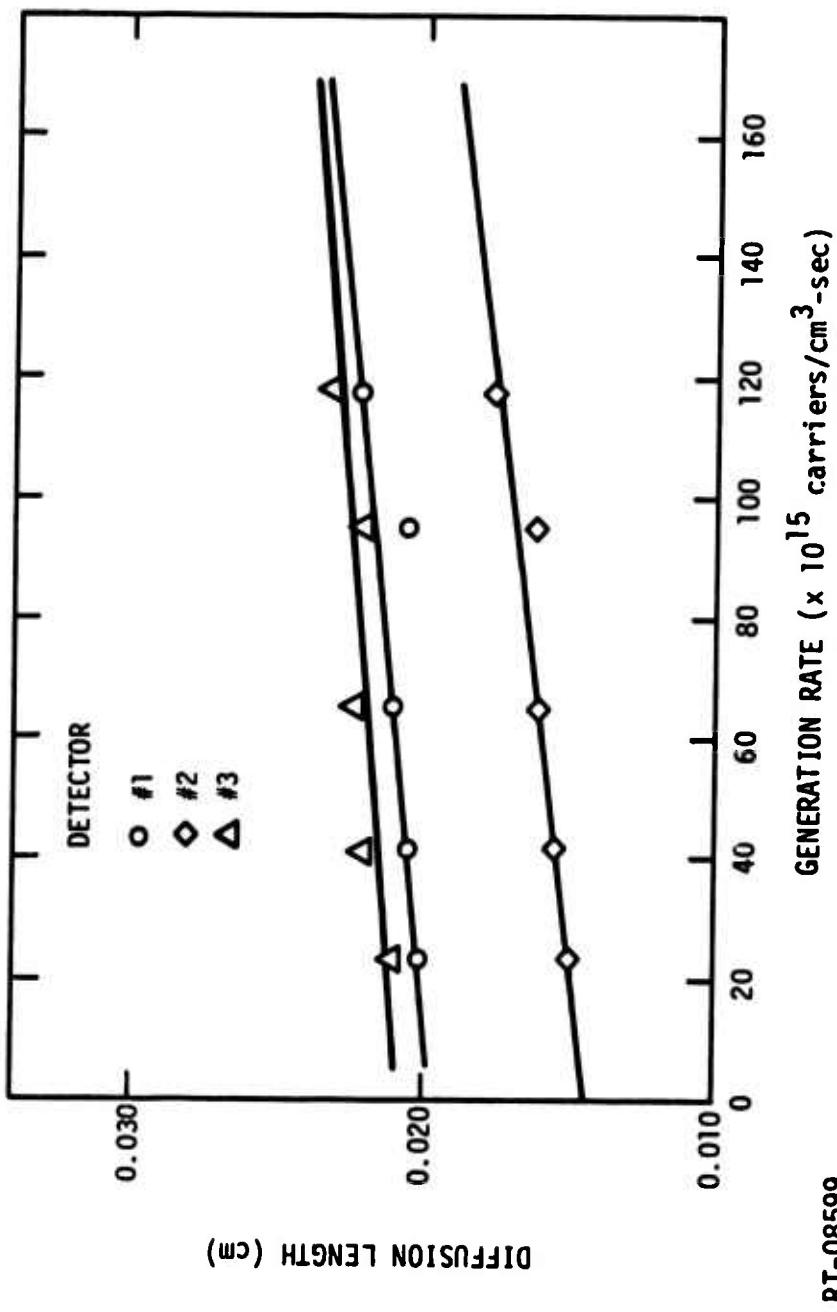
Figure 30. Diffusion lengths as a function of generation
rate, steady state, silicon filter

RT-08599

57

mobility of 1400 cm^2/V-sec, the corresponding minority-carrier lifetime is

$$\tau = \frac{L_b^2}{(kT)\mu} = \frac{(0.02)^2}{(0.025)(1400)} = 11.4 \text{ } \mu sec \text{ .}$$

This lifetime is more than an order of magnitude shorter than the initial base value (Table 2). Since the apparent diffusion length (∿0.02 cm) is close to the estimated thickness of the detector (0.025 to 0.029 cm), essentially all of the carriers generated in the detector are collected for the short-circuit current. Therefore, the lifetime (11.4 μsec) calculated from this current is only a lower limit and the lifetime might well be closer to the value quoted by the manufacturer (Table 2).

In the transient measurements (Section 4.6), an apparent decay time of ∿1 μsec is observed, but this value is obtained with fairly highly absorbed light. Therefore, the resulting decay time would be influenced by the sweep-out time of the diffused junction.

4.4 Reverse-Bias Dependence

Using the silicon-filtered light source, the reverse-bias dependence of the rms response to the penetrating light was measured, and the results are shown in Figure 31. Since the effective active region of the detector with zero bias is essentially the full volume of the detector, one would not expect much increase in the response with reverse bias, as illustrated in Figure 31. The slight increase with bias is undoubtedly a sweep-out effect where the sweep-out time is made much less than the recombination time. At higher values of bias, the dark current in uncapped detectors 2 and 3 became quite large, probably because of enhanced edge effects due to handling and atmospheric effects.

4.5 Depletion-Layer Capacitance

Measurements of the detector capacitance as a function of reverse bias were performed using a Hewlett-Packard model 4270A capacitance bridge. The measurements were made at a frequency of 1 MHz using the instrument's

58
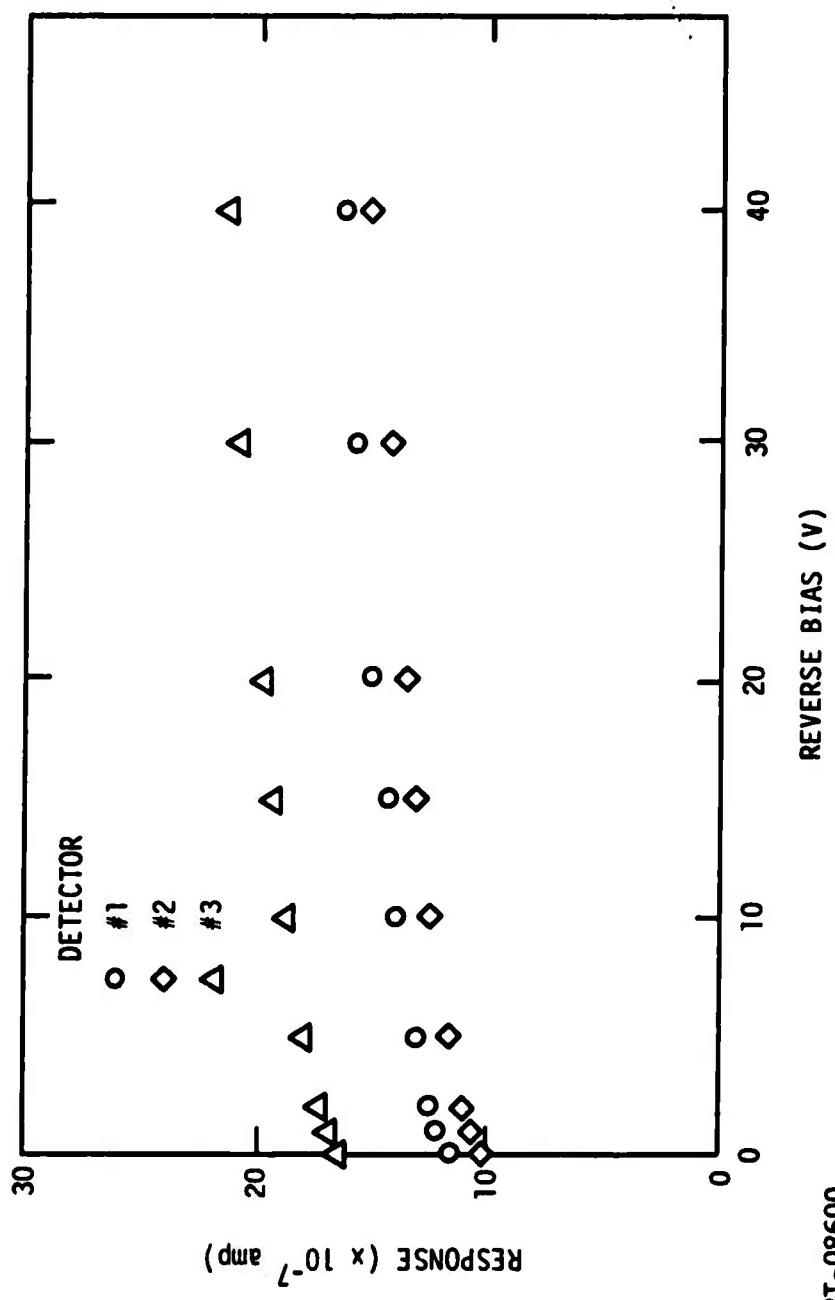
Figure 31.   Detector response to penetrating light as a function of reverse bias, silicon filter, f = 100 Hz

RT-08600

oscillator voltage of ∿10 mV rms. An external dc power supply was used to provide the dc bias.

Assuming an abrupt, one-sided junction (that is, one side much more heavily doped than the other), the capacitance per unit area is given by

$$C = \left[\frac{q \epsilon N_e}{2(V_{Bi} + V)} \right]^{\frac{1}{2}} \; .$$

Thus, plotting $1/C^2$ as a function of the reverse-bias voltage should yield a straight-line relationship for an abrupt junction; the voltage intercept of the curve at $1/C^2 = 0$ gives the value of the built-in potential. The slope of the line is inversely proportional to the doping density N_e on the lightly doped side.

Figure 32 shows the quantity $1/C^2$ plotted against the reverse bias for two cases: curve A corresponds to the dark detector and curve B corresponds to the detector with a small amount of illumination falling on it. The most obvious effect of the low-level illumination is to move the intercept at $1/C^2 = 0$, indicating a displacement of the quasi-Fermi levels due to the excess carriers generated. At very high levels of illumination, the equation is no longer valid due to the extreme distortion of the field across the device.

For small values of bias, the straight-line fit is fairly good. Using the straight-line fit to the curve for no illumination, the intercept at $1/C^2 = 0$ gives a value of ∿0.45 volt for the built-in voltage; the slope of the straight line, 2.82×10^{17} cm^4/farad^2-volt, is used to calculate a value of 3.6×10^{13} cm^{-3} for the impurity concentration in the substrate material. This value is in good agreement with the value of 3.9×10^{13} cm^{-3} from the manufacturer's specifications (340 ohm-cm, p-type).

Curves A and B are the best-fit curves for the low-bias region; the data points over higher values of bias fit a $1/C^{2.3}$ relation, which indicates that the junction is not abrupt as originally assumed.

Using the calculated values for V_{Bi} and N_e in the approximate relation for depletion-layer width for an abrupt junction,

$$W = \left[\frac{2 \epsilon V_{Bi}}{q N_e} \right]^{\frac{1}{2}} \; ,$$
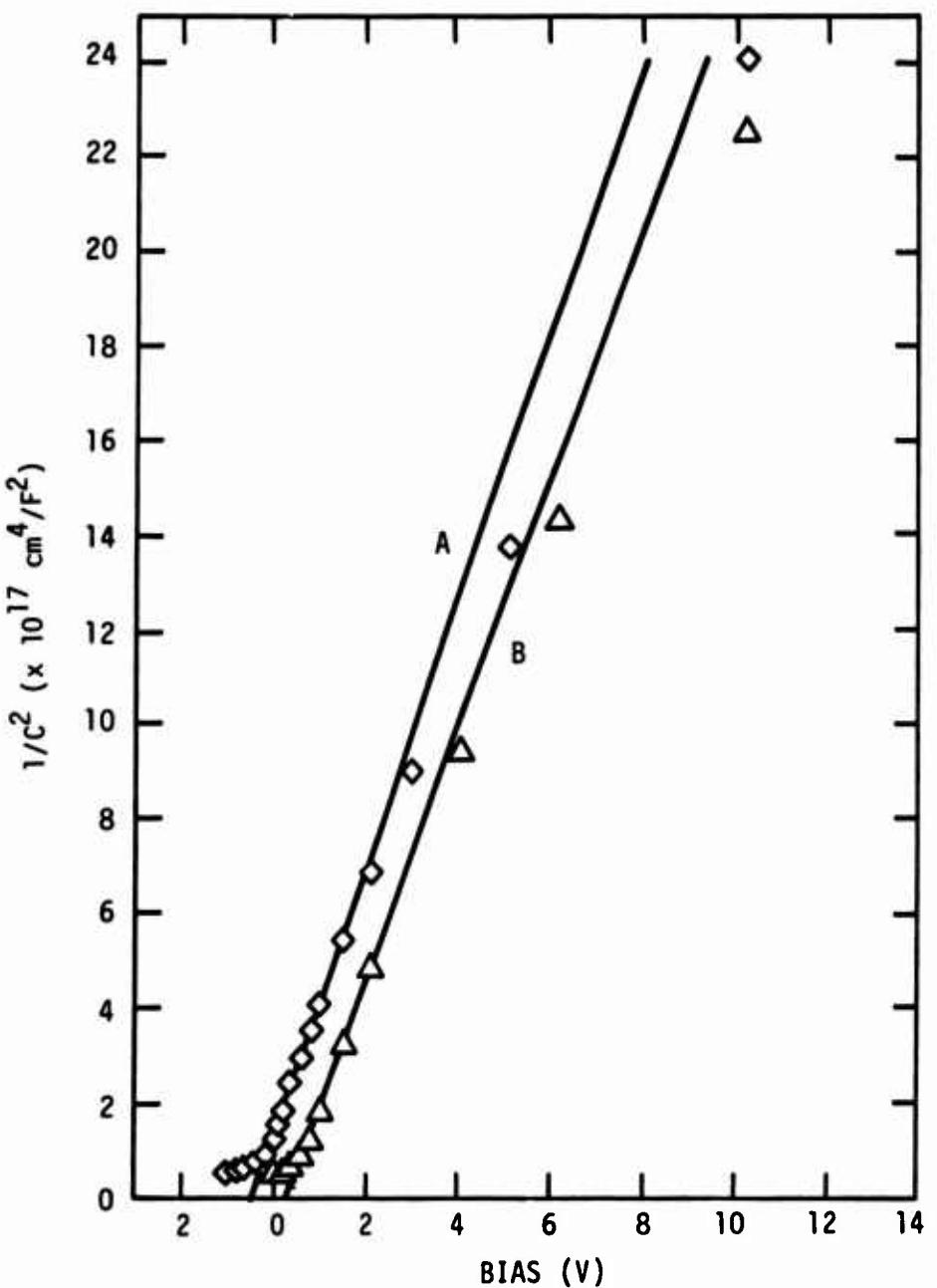
Figure 32. Value $1/C^2$ as a function of reverse bias; curve A, dark detector; curve B, low-level illumination on detector

a junction width of 3.7×10^{-4} cm is calculated. The calculated width is about a factor of 4 more than was expected for these detectors, based on an estimate of 1 to 2 μm provided by the manufacturer's representative.

4.6 Transient Measurements

To obtain some transient response data for comparison to model results, a GaAs laser with a pulse width of 15 μsec was used to excite one of the detectors. Figure 33a shows a reproduction of a typical oscilloscope trace during the first exploratory experiments with the detector. When the reverse bias was increased, the height of the prompt response during the pulse increased and the component after the pulse decreased. At that time, it was thought that the response af er th pulse was the usual diffusion current from the base. It appeared th.. .creasing the reverse bias increased the depletion width and, therefore, the prompt current. Since the device is fairly narrow, as the depletion width increased the remaining distance from which the diffusion current would arise was decreased, so the diffusion current would also decrease. One difficulty with this explanation is that the delayed current did not decay with a simple exponential, as one might expect for a diffusion current.

After the other measurements described in the previous sections were completed, an attempt was made to duplicate these first transient runs. For some unexplained reason, the type of response illustrated in Figure 33a could not be reproduced on any of the three detectors using the same GaAs laser. Instead, the responses were as shown in Figure 33b. The main difference was the absence of the sharp decrease in signal coincident with the end of the pulse. These results have since been repeated a number of times with similar results. The following are some possible reasons for these differences, although they are just speculations at this time. The first responses could have been some artifact of the electronic circuit, although this seems unlikely because the response was so rapid and so well coordinated with the laser pulse. The first detector may have been degraded between the first and second set of experiments. Again, this seems unlikely because all three detectors gave similar results during the second set of experiments. At present, the most likely source of the difference seems to be that the

62
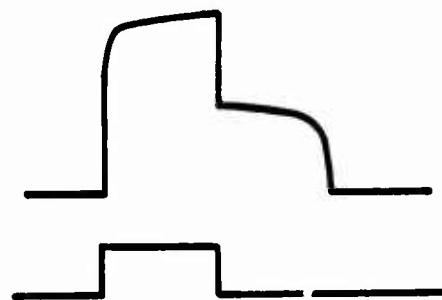
a. Typical results during first exploratory experiments
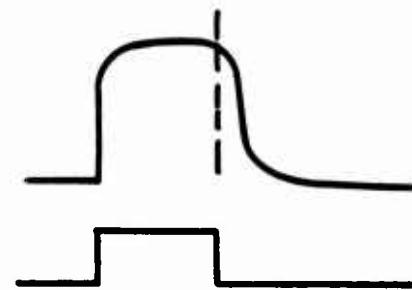
RT-08602

b. Typical results from repeated experiments

Figure 33. Reproduction of oscilloscope traces; upper beam, voltage
across load resistor as a function of time; lower beam,
voltage proportional to light intensity emitted by GaAs
laser; gains in arbitrary units; light pulse width 15 μsec

63

intensity of the GaAs laser was degraded between the two sets of experiments because it had been used for other experiments in the interval. Thus, the drop in signal at the end of the pulse may be related to the intensity of the excitation.

During the second experiments, it was found that the delayed current was a function not only of the applied bias but also of the exterior load resistance and the intensity of the illumination. For a given excitation level and a small reverse bias (-50 mV), the response with a load of 750 ohms was similar to Figure 33b. However, when the load was decreased to ∿50 ohms or the reverse bias was increased, the delayed current dropped off rapidly with a time constant of around 1 μsec. Thus, the effective life-time of this device, when it is illuminated with the GaAs laser, is appar-ently much less than the value (∿11 μsec) calculated from the short-circuit current (Section 4.3) or the range of values (200 to 350 μsec) quoted by the manufacturer (Table 2) for the initial bulk material. Since the light from the GaAs laser is attenuated to about 0.2 of its incident value in 30 μm in silicon, this decay lifetime is representative only of the first 30 μm of the detector. With a diffused junction, the built-in fields might extend over most of this distance and the observed decay time may be domi-nated by carrier sweep-out.

The fact that the response illustrated in Figure 33b is a function of load, light intensity, and applied bias undoubtedly means that this delayed component is similar to the currents in a transistor when it is first switched from the saturated condition. When this occurs, the current remains essentially constant during the storage delay time, and then it decreases similar to Figures 33a and b. The conditions that give rise to currents of this type are probably not representative of good detector operation. There-fore, if this explanation is correct, this phenomenon is not too important for this program, except that it must be understood to plan the experimental program and interpret the results.

4.7 Discussion of Measurements on Photovoltaic Detectors

The capacitance-voltage measurements yielded reasonable values for the built-in voltage and the doping density in the base. However, the lifetime

calculated from the short-circuit current is less than the initial bulk value quoted by the manufacturer, is approximately equal to the detector thickness, and is larger than the apparent decay lifetime following excitation by a GaAs laser. However, the latter time may be primarily the sweep-out time for the diffused junction.

Now that we apparently better understand the results from the transient measurements, these experiments should be repeated using a calibrated, more penetrating light source and a careful choice of biases and load resistances to obtain both the decay time and the saturated currents. These results should then be verified by simulating the same conditions on the PN code to make sure that our explanation is correct.

5. PLANS FOR COMING YEAR

The plans for the coming year are to use the model for the silicon
photoconductive detector to study other aspects of their response; for
example, how important are the particular boundary conditions used in the
PN code, and what would be the effect of vastly different boundary condi-
tions? This basic model will also be used to try to reproduce the observed
spiking results and determine, if possible, what factors influence the
spiking. The present silicon photovoltaic detector will be modeled and
compared to the data in this report and any additional results that may
be obtained. The manufacturer's specifications on various photovoltaic
detectors will be reviewed to see if some other device might have charac-
teristics that would be more useful to model than the present detectors.
And finally, a start will be made on modeling trimetal detectors.

REFERENCES

1. R. E. Leadon et al., "Analysis of the Performance of IR Detectors Under Radiation Environment," INTEL-RT 8028-002, Scientific Report No. 1, July 25, 1973.

2. P. Norton et al., "Carrier Lifetime and Mobility in n-Type Silicon," presented at IRIS Specialty Group on Infrared Detectors, Washington, D.C., March 1973.

3. M. Lax, Phys. Rev. 119, 1502 (1960).

4. E. J. Ryder, Phys. Rev. 90, 766 (1953).

5. For example, 1974 IRIS Detector Specialty Group Meeting, Marine Corps Air Station, El Toro, California, March 5-7, 1974.